Hypothalamic bile acid-TGR5 signaling protects from obesity

Ashley Castellanos-Jankiewicz[1#], Omar Guzmán-Quevedo[1,2,3#¤], Valérie S. Fénelon[1], Philippe Zizzari[1], Carmelo Quarta[1], Luigi Bellocchio[1], Anne Tailleux[4], Julie Charton[5], Daniela Fernandois[6], Marcus Henricsson[7], Catherine Piveteau[8], Vincent Simon[1], Camille Allard[1], Sandrine Quemener[4], Valentine Guinot[4], Nathalie Hennuyer[4], Alessia Perino[9], Alexia Duveau[1], Marlène Maitre[1], Thierry Leste-Lasserre[1], Samantha Clark[1], Nathalie Dupuy[1], Astrid Cannich[1], Delphine Gonzales[1], Benoit Deprez[5], Gilles Mithieux[10], David Dombrowicz[4], Fredrik Bäckhed[7,11,12], Vincent Prevot[6], Giovanni Marsicano[1], Bart Staels[4], Kristina Schoonjans[9], Daniela Cota[1*]

[1]University of Bordeaux, INSERM, Neurocentre Magendie, U1215, F-3300 Bordeaux, France; [2]Laboratory of Neuronutrition and Metabolic Disorders, Instituto Tecnológico Superior de Tacámbaro, 61650 Tacámbaro, Michoacán, Mexico; [3]Pós-Graduação em Neuropsiquiatria e Ciências do Comportamento, Universidade Federal de Pernambuco, 50732-970 Recife, Pernambuco, Brazil; [4]INSERM U1011, University of Lille-EGID; CHU Lille; Institut Pasteur de Lille, 59019 France; [5]University of Lille, INSERM, Institut Pasteur de Lille, U1177 - Drugs and Molecules for living Systems, EGID, F-59000 Lille, France; [6]University of Lille, INSERM, CHU Lille, Laboratory of Development and Plasticity of the Neuroendocrine Brain, Lille Neuroscience & Cognition, UMR-S1172, EGID, F-59000, Lille, France; [7]The Wallenberg Laboratory, Department of Molecular and Clinical Medicine, Institute of Medicine, Sahlgrenska Academy, University of Gothenburg, 413 45 Gothenburg, Sweden; [8]University of Lille, INSERM, Institut Pasteur de Lille, U1177 - Drugs and Molecules for living Systems, F-59000 Lille, France;[9]Institute of Bioengineering, Faculty of Life Sciences, Ecole

Polytechnique Fédérale de Lausanne, 1015 Lausanne, Switzerland; [10]INSERM U1213 Nutrition, Diabetes and the Brain, University of Lyon 1 Faculté de Médecine Lyon-Est, 69372 Lyon, France;[11]Novo Nordisk Foundation Center for Basic Metabolic Research, Faculty of Health Sciences, University of Copenhagen, 2200 N Copenhagen, Denmark;[12]Region Västra Götaland, Sahlgrenska University Hospital, Department of Clinical Physiology, Gothenburg, Sweden.

***Correspondence and Lead contact:** daniela.cota@inserm.fr

[#] These authors contributed equally

[¤]Present address: Laboratory of Neuronutrition and Metabolic Disorders, Instituto Tecnológico Superior de Tacámbaro, 61650 Tacámbaro, Michoacán, Mexico.

Summary

Apart from emulsifying lipids, bile acids (BA) improve metabolism and exert anti-obesity effects through the activation of the Takeda G protein-coupled receptor 5 (TGR5) in peripheral tissues. TGR5 is also found in the brain hypothalamus, but whether hypothalamic BA signaling is implicated in body weight control and in obesity pathophysiology remains unknown. Here we show that central administration of BA or of a specific TGR5 agonist in diet-induced obese mice decreases body weight and fat mass by activating the sympathetic nervous system, thereby promoting negative energy balance. Conversely, genetic downregulation of hypothalamic TGR5 expression in the mediobasal hypothalamus favors the development of obesity and worsens established obesity by blunting sympathetic activity. Lastly, hypothalamic TGR5 signaling is required for the anti-obesity action of dietary BA supplementation. Together, these findings identify hypothalamic TGR5 as a key mediator of a top-down neural mechanism that counteracts obesity.

Keywords

Obesity, hypothalamus, TGR5, bile acids, food intake, body weight, energy expenditure, sympathetic nervous system

Introduction

Bile acids (BA) are cholesterol-derived molecules produced by the liver that exert hormone-like metabolic effects (Kuipers et al., 2014; Perino et al., 2020) by binding to the nuclear farnesoid X receptor (FXR) and to the membrane-bound Takeda G protein-coupled receptor 5 (TGR5) (Kuipers et al., 2014; Perino et al., 2020), which are both expressed in peripheral organs. BA-dependent activation of hepatic FXR inhibits BA synthesis, regulates lipid and glucose metabolism and contributes to hepatic gluconeogenesis, among other effects (Kuipers et al., 2014; Perino et al., 2020). Whilst, BA activation of TGR5 in intestinal L-cells and pancreatic β-cells stimulates the release of glucagon-like peptide-1 (GLP-1) and insulin, respectively, thereby improving glucose homeostasis (Kumar et al., 2012; Thomas et al., 2009). In monocytes and macrophages, TGR5 activation inhibits pro-inflammatory responses in the adipose tissue of mice fed a high-fat diet (HFD) (Perino et al., 2014). Of interest, dietary supplementation of specific BA, such as cholic acid (CA) or chenodeoxycholic acid (CDCA), prevents weight gain and leads to significant weight loss in diet-induced obese (DIO) mice, mainly through an increase in thermogenesis and energy expenditure (Teodoro et al., 2014; Watanabe et al., 2006). Circulating BA levels also correlate with energy expenditure in healthy humans (Ockenga et al., 2012) and with changes in energy and substrate metabolism in obese subjects undergoing Roux-en-Y gastric bypass surgery (Patti et al., 2009; Simonen et al., 2012). Mechanistically, activation of TGR5 by BA increases thermogenesis in mouse and human brown adipocytes by promoting intracellular thyroid hormone activation through type 2 iodothyronine deiodinase (D2) and by stimulating mitochondrial respiration (Broeders et al., 2015; Watanabe et al., 2006). Besides, TGR5 activation in white adipocytes

participates in the beiging process by increasing β-oxidation and improving mitochondrial function (Velazquez-Villegas et al., 2018).

While these findings suggest a role for peripheral BA-TGR5 signaling in counteracting DIO, neuronal circuits located in the mediobasal hypothalamus (MBH) are known to regulate energy expenditure, thermogenesis and food intake (Clapham, 2012; Dietrich and Horvath, 2013) and may therefore contribute to BA-mediated effects on energy balance. Several pieces of evidence support this possibility: i) BA are found in the brain, where their levels correlate with circulating ones (Higashi et al., 2017; Parry et al., 2010); ii) under acute cholestasis, BA rapidly accumulate in the hypothalamus (Doignon et al., 2011); iii) TGR5 is expressed in the brain of rodents (Doignon et al., 2011; Maruyama et al., 2006) and humans (Kawamata et al., 2003), and it is found in neurons, astrocytes and microglia (Keitel et al., 2010; McMillin et al., 2015; Zuo et al., 2019). Nevertheless, whether hypothalamic BA-TGR5 signaling is implicated in energy balance and obesity pathophysiology remains unknown.

By using both pharmacological and genetic approaches combined with metabolic phenotyping, we show that activation of central TGR5 signaling counteracts DIO, whereas genetic downregulation of hypothalamic TGR5 promotes it. These effects, which involve modulation of food intake and of energy expenditure through the sympathetic nervous system (SNS), reveal that a long-range BA-dependent hypothalamic mechanism contributes to weight regulation and peripheral metabolic improvements under DIO.

Results and Discussion

Central TGR5 agonism counteracts obesity

To determine whether DIO alters peripheral or brain BA levels, we quantified circulating and hypothalamic BA in the post-prandial state (2h after re-exposure to food following a 24h fast) in both chow lean and DIO mice. Total plasma levels were not significantly different (Figure 1A and Table S1), but total hypothalamic BA levels were reduced in DIO mice as compared to lean controls (Figure 1B). Changes in specific BA species were further observed in both plasma and hypothalamus of obese mice (Figure 1A and 1B). In particular, significant decreases in deoxycholic acid (DCA), taurodeoxycholic acid (TDCA), and taurocholic acid (TCA), which all act as TGR5 agonists (Kawamata et al., 2003), were detected in the hypothalamus of DIO mice (Figure 1B). Hypothalamic and plasma levels of the potent TGR5 agonist DCA, but not TDCA or TCA, significantly correlated (Figure 1C). Since BA can both diffuse and potentially be actively transported into the brain (Mertens et al., 2017), we evaluated changes in the hypothalamic mRNA expression of different BA transporters after 2h refeeding, as compared to 24h fasting. Food intake tended to increase the expression of all BA transporters, with a significant effect observed for the bile salt export pump (Bsep) in chow, but not DIO animals (Figure 1D). In parallel, food intake reduced hypothalamic TGR5 expression in lean controls, but not in DIO mice (Figure 1D). Thus, DIO leads to a decrease in the hypothalamic content and possibly in the signaling activity of BA species that act as TGR5 agonists, particularly in response to changes in energy availability.

Next we tested whether central pharmacological activation of TGR5 affects food intake and/or body weight under obesogenic conditions. DIO mice were acutely treated with an intracerebroventricular (icv) injection of the synthetic TGR5-specific agonist 3-(2-Chlorophenyl)-N-(4-chlorophenyl)-N,5-dimethyl-4-isoxazolecarboxamide (CCDC) (Evans et al., 2009; Jensen et al., 2013). After excluding leakage of CCDC into the

periphery (Table S2), we evaluated the effect of increasing icv doses of CCDC, which were administered just before the onset of the dark phase, in 24h-fasted DIO mice. Acute administration of CCDC (5μg dose), significantly reduced food intake over time, with a robust reduction in 24h food intake and body weight gain as compared to vehicle-treated animals (Figure 1E and 1F). Similar effects were observed after icv administration of a mix of BA acting as TGR5 agonists (Figure 1G and 1H and Figure S1A) as well as after delivery of CCDC in the MBH (Figure S1B and S1C).

Based on these findings, we studied the impact of 4 weeks icv administration of the drug (5μg/day) on body weight in DIO mice. A robust reduction in body weight (Figure 1I) and fat mass (Figure 1J) was observed, with no changes in lean mass (Figure 1K). Central CCDC administration also reduced food intake (Figure 1L and S1D) and improved insulin responsiveness (Figure 1M and S1E). Importantly, CCDC was undetectable in plasma (Table S2), thereby demonstrating its brain-restricted action. Feed efficiency was also reduced by central CCDC treatment (Figure 1N), implying that mechanisms other than reduced food intake contribute to the observed anti-obesity action. Of note, the central anti-obesity action of CCDC was specific to DIO, since chronic central administration of the drug did not affect body weight, food intake, or body composition in genetically obese ob/ob mice (Figure 1O-R).

Chronic central TGR5 agonism recruits the sympathetic nervous system

To address whether changes in energy expenditure contribute to CCDC-mediated weight loss in DIO mice (Figure 1I), we performed indirect calorimetry analysis in a new cohort of animals before treatment-induced differences in body weight became significant. Mice receiving chronic icv CCDC had increased energy expenditure during

the dark phase (Figure 2A and S2A), and a significant overall daily decrease in respiratory exchange ratio (RER), suggesting preferential use of lipids as energy substrate (Figure 2B), with no changes in locomotor activity (Figure 2C and S2C). The increase in energy expenditure and the reduction in RER were blunted in the same CCDC-treated animals at thermoneutrality (Figure 2A, S2A and S2B), suggesting that chronic central TGR5 activation could be increasing SNS activity. However, there was no significant difference in meal size between the treatments groups (Figure S2D and S2E). Furthermore, mRNA expression of β1, 2 and 3 adrenoreceptors (AR), which regulate thermogenesis and lipolysis (Blaszkiewicz and Townsend, 2016; Clapham, 2012) and Dio-2 (the gene expressing the deiodinase enzyme D2), were increased respectively in the epidydimal WAT and BAT from CCDC-treated DIO mice at standard housing temperature (22°C, Figure 2D and 2E), but unchanged at thermoneutrality (30°C, Figure 2F and 2G).

Long-range brain-to-periphery mechanisms control hepatic BA production, at least under conditions in which high BA levels may become toxic for the organism (Doignon et al., 2011). To address whether the observed increase in energy expenditure might have been due to brain-to periphery feedback loops affecting circulating BA, we evaluated plasma BA profiles after 10 days and 4 weeks of continuous icv CCDC administration in DIO mice. No changes in plasma total or specific BA species were observed after 10 days (Figure S2F) or 4 weeks (data not shown) of icv CCDC administration, suggesting that top-down neuronal pathways must mediate the phenotypic changes observed. To this end, we studied whether the SNS contributes to CCDC-mediated effects, by performing chemical sympathectomy with 6-hydroxydopamine (6-OH-DOPA), which blunted the expression of the rate limiting enzyme for catecholamine synthesis tyrosine hydroxylase (TH) (Vaughan et al., 2014),

by 77.5% in epidydimal WAT and 46.6% in BAT (Figure S2G). Sympathectomy reversed the previously described effects (see Figure 1I-L) of chronic icv CCDC treatment on body weight, body composition and food intake (Figure 2H-K). Thus, chronic central TGR5 agonism reduces adiposity by stimulating SNS activity in DIO mice.

TGR5 activity in the mediobasal hypothalamus protects from obesity

To uncover the role of hypothalamic TGR5 in obesity pathophysiology, we selectively deleted TGR5 in the MBH of TGR5$^{f/f}$ mice (Thomas et al., 2009) via stereotaxic injection of AAV-Cag-Cre-GFP viral particles or control viruses (AAV-Cag-GFP). A group of C57BL/6J mice receiving AAV-Cag-Cre-GFP was also used to exclude potential Cre-mediated off-target effects. The viral strategy employed targeted neurons rather than astrocytes or microglia (Figure S3A), and led to Cre recombination (Figure S3B) and a ~50% reduction of TGR5 mRNA expression specifically in the MBH, but not in other brain regions (Figure S3C), demonstrating the validity of the approach.

Notably, once exposed to HFD, TGR5$^{f/f}$-AAV-Cag-Cre-GFP mice gained more weight than TGR5$^{f/f}$-AAV-Cag-GFP or C57BL/6J-AAV-Cag-GFP controls (Figure 3A). TGR5$^{f/f}$-AAV-Cag-Cre-GFP mice also showed increased fat mass relative to control groups (Figure 3B), with no changes in lean mass (Figure 3C), modest hyperphagia (Figure 3D and S3D) and higher feed efficiency (Figure 3E). Strikingly, when AAV-mediated hypothalamic TGR5 knockdown was carried out in already DIO TGR5$^{f/f}$ mice, a further increase in body weight (Figure 3F), fat mass (with no changes in lean mass, Figure 3G and 3H), food intake (Figure 3I and S3E) and feed efficiency (Figure 3J) was

observed, demonstrating that loss of hypothalamic TGR5 promotes the onset and worsening of DIO.

The increased feed efficiency observed in TGR5$^{f/f}$-AAV-Cag-Cre-GFP mice led us to hypothesize that hypothalamic TGR5 signaling may affect peripheral energy metabolism via changes in SNS-dependent thermogenesis. Accordingly, when HFD-fed TGR5$^{f/f}$-AAV-Cag-Cre-GFP and control mice were acutely exposed to a cold challenge (4°C for 4 hours), which activates the SNS (Clapham, 2012), TGR5$^{f/f}$-AAV-Cag-Cre-GFP mice displayed decreased protein expression of the thermogenic marker UCP-1 in the BAT (Figure 3K), decreased SNS-dependent phosphorylation of the lipolysis marker hormone sensitive lipase (HSL) in the WAT (Figure 3L), and blunted mRNA levels of molecular markers of thermogenesis, fatty acid use and glucose clearance, such as β3-AR, HSL, insulin receptor (Insr), solute carrier family 2 member 4 (Slc2a4) and peroxisome proliferator activated receptor alpha (PPARα) in this tissue (Figure 3M). Thus, reducing hypothalamic TGR5 expression hinders SNS activity, possibly leading to a higher DIO sensitivity. Accordingly, at thermoneutrality (30°C), the phenotype of TGR5$^{f/f}$-AAV-Cag-Cre-GFP exposed to HFD was undistinguishable from controls (Figure 3 N-R).

Characterization of hypothalamic cell types implicated in TGR5-mediated effects on energy balance

To uncover possible hypothalamic cell-types implicated in the TGR5 action on body weight control, we characterized the molecular identity of TGR5-expressing hypothalamic cells, using a TGR5-promoter-driven reporter model (Figure S3F). FACS-sorting of hypothalamic cells was followed by qPCR of markers of neuronal

populations known to influence energy balance. Enrichment of mRNA expression for specific neuropeptides (NPY, POMC, SF1), neurotransmitters transporters (vGat, vGlut2), enzymes (TH, GAD1, GAD2), and hormone receptors (leptin receptor, LepR) was observed in TGR5-positive relative to TGR5-negative cells (Figure 3S and S3F). To corroborate these findings, we quantified TGR5 mRNA levels in specific sup-populations of GABAergic (vGat-positive) and glutamatergic (vGlut2-positive) hypothalamic neurons. To achieve this, we employed laser capture microdissected analysis of individual fluorescent cells obtained from vGat-ires-Cre and vGlut2-ires-Cre mice, which were stereotaxically injected with an pAAV-hSyn-DIO-mCherry in the MBH (Figure S3G). Comparable TGR5 mRNA levels were observed in both GABAergic and glutamatergic neurons (Figure S3H), suggesting that both neuronal populations may contribute to the phenotypes observed after AAV-based deletion of hypothalamic TGR5. Accordingly, the viral-mediated model used to delete TGR5 led to Cre-mediated recombination in ~36.7% of GABAergic and ~39.8% of glutamatergic neurons (Figure 3T).

To finally confirm that the metabolic effects observed *in vivo* stem from hypothalamic neurons rather than from non-neuronal cells expressing the receptor, we targeted the expression of TGR5 in MBH astrocytes by using an AAV-Cre-mCherry expressing the Cre recombinase under the control of the promoter for the astrocytic gene glial fibrillary acidic protein (GFAP). Although this approach led to specific Cre expression in GFAP-positive cells (Figure S4A), to genomic TGR5 recombination (Figure S4B), and decreased hypothalamic TGR5 mRNA levels (Figure S4C), no changes in body weight, body composition, food intake, or feed efficiency were observed in these animals (Figure S4 D-H).

Hypothalamic TGR5 signaling contributes to the anti-obesity action of BA supplementation

Dietary supplementation with CA, its synthetic derivatives or other BA acting as TGR5 agonists reduce weight gain by increasing thermogenesis and energy expenditure (Thomas et al., 2009; Watanabe et al., 2006; Zietak and Kozak, 2016). As dietary supplementation with CA results in a significant, supraphysiological increase in circulating BA levels (Song et al., 2011; Watanabe et al., 2006) likely reaching the brain, we asked whether hypothalamic TGR5 signaling contributes to the therapeutic effects exerted by the systemic delivery of TGR5 agonists. To test this hypothesis, TGR5$^{f/f}$-AAV-Cag-Cre-GFP mice and their TGR5$^{f/f}$-AAV-Cag-GFP controls were fed with a HFD, supplemented or not with 0.5% CA, as in (Watanabe et al., 2006). CA supplementation prevented body weight gain over time in the controls (Figure 4A) and reduced food intake (Figure S5A and S5B), body weight and fat mass as well as feed efficiency by the end of the study (Figure S5 C-E). The decreased food intake (Figure S5A and S5B) was not due to aversion, since a food preference test showed that when having the choice, mice would eat the HFD supplemented with CA rather than chow (Figure S5F). Knockdown of hypothalamic TGR5 increased body weight, fat mass, food intake and feed efficiency in both HFD-fed and HFD-CA fed mice (Figure 4A and S5 A-E). We then calculated CA-induced fold changes of these parameters and observed that the degree of efficacy of CA supplementation in reducing body weight, fat mass and feed efficiency was strongly diminished in mice with hypothalamic TGR5 knockdown (Figure 4B, 4C and 4E). Whilst, hypothalamic TGR5 knockdown only tended to hinder ($p=0.06$) the CA-induced decrease on food intake (Figure 4D). Thus, systemic administration of TGR5 agonists, here through dietary supplementation with CA, requires functional hypothalamic TGR5 to efficiently prevent weight gain.

In conclusion, our work demonstrates that hypothalamic TGR5 as a key regulator of food intake and of SNS-driven effects on body weight through adipose signaling, and offers a new foundation for understanding the mechanisms involved in the anti-obesity efficacy of pharmacological strategies that modulate the BA-TGR5 pathway. Our neuroanatomical and molecular studies revealed that both glutamatergic and GABAergic neurons expressing TGR5 may be involved, further demonstrating that MBH TGR5-positive cells express molecular markers of specific neuronal types implicated in energy balance regulation. Differently, although hypothalamic astrocytes play a role in obesity pathophysiology (García-Cáceres et al., 2019), TGR5 on this specific cell population is not involved in this context. Further studies will have to determine whether TGR5 may modulate inflammatory or immune responses in glia, as already demonstrated in peripheral immune cells (Perino et al., 2014). Our data reveal that both central and peripheral TGR5 signaling contributes to body fat loss under obesogenic conditions and that brain-selective activation of TGR5 effectively reduces food intake, while downregulation of the receptor causes hyperphagia. However, TGR5 expressed in the periphery can also contribute to the regulation of feeding. Indeed, supplementation of CA in HFD can still reduce food intake in mice with hypothalamic TGR5 knockdown. Accordingly, BA stimulate satiety through activation of TGR5 in the nodose ganglia neurons (Wu et al., 2020), whereas other studies have shown that BA-mediated metabolic effects involve a gut-to-brain axis (Liu et al., 2018).

We now provide evidence of a hypothalamic BA-TGR5 pathway that is relevant for top-down regulation of body weight under obesogenic conditions. This implies that bidirectional brain-periphery mechanisms are engaged by BA to control metabolic

responses at multiple levels. With the present evidence, we propose a shift in the current view of BA metabolic actions, which should now include a central perspective.

Limitations of Study

While our study showed a critical role for hypothalamic TGR5 as defense mechanism against diet-induced obesity, which participates to the weight-lowering action of systemic TGR5 agonists, our work has some limitations. Our genetic approach and neuroanatomical and molecular studies, while providing information on different type of neurons potentially involved, do not allow pinpointing the exact neuronal population(s) driving the observed effects. More studies are needed to investigate the underlying neuronal circuitry engaged by TGR5 and its relevance to the human condition.

Acknowledgements

We thank the animal housing, genotyping, transcriptomic, laser capture microdissection, and bioinformatics facilities of INSERM U1215 Neurocentre Magendie, funded by INSERM, LabEX BRAIN ANR-10-LABX-43 and FRM DGE20061007758 for animal care, cells microdissection, genotyping and qPCR studies. We thank the biochemistry and biophysics facility of the Bordeaux Neurocampus funded by the LabEX BRAIN for western blot equipment. The microscopy was done in the Bordeaux Imaging Center, a service unit of the CNRS-INSERM and Bordeaux University, member of the national infrastructure France BioImaging supported by the LabEX BRAIN. We thank Dr. C. Herry (INSERM U1215) for the use of the vGlut2-ires-Cre mouse line, E. Huc (INSERM U1215) for breeding of

our mice colonies, Nathalie Jouy (UMS2014-US41, University of Lille) and G. Ferretti (University of Bologna) for technical help, and C. Padgett for artwork.

Supported by INSERM (D.C., C.Q., G.Ma., L.B.), Aquitaine Region (D.C., G.Ma.), ANR-13-BSV4-0006 NeuroNutriSens (D.C., G. Ma.), ANR-17-CE14-0007 BABrain (D.C., G.Mi., B.S., B.D.), Labex BRAIN ANR-10-LABX-43 (D.C., G.Ma.); ANR-10-EQX-008-1 OPTOPATH (D.C.), ANR-18-CE14-0029 MitObesity (D.C., G.Ma.), ANR-20-CE14-0046, French Societies of Endocrinology (SFE), Nutrition, and Diabetes (SFE, SFN and SFD) (C.Q.) and Fondation Francophone pour la Recherche sur le Diabète (FFRD) (D.C., G.Mi.), which is sponsored by Fédération Française des Diabétiques (AFD), AstraZeneca, Eli Lilly, Merck Sharp & Dohme, Novo Nordisk, and Sanofi. Mexican CONACYT PhD fellowship (A.C-J.), Mexican CONACYT post-doc fellowship (O. G-Q.), AXA post-doctoral fellowship (A.P.), PhD extension grant LabEX BRAIN (A.C-J.), an ERC Synergy Grant WATCH (810331, V.P.), an ERC Advanced Grant (694717, B.S.) and Labex EGID ANR10-LABX-46 (B.S.), Swiss National Science Foundation (SNSF N° 310030_189178, K.S.) and KG Jebsen Foundation (K.S.).

Author contributions

A.C-J., O.G-Q., V.S.F., P.Z., C.Q., L.B., A.T. J.C., D.F. M.H., C. P., V.S., C.A., S.Q., V.G., N. H., A.D., M.M., T. L-L., S.C., N.D., A.C., D.G. generated the data; A.C-J., O.G-Q., V.S.F., P.Z., A.T., J.C., D.F., M.H., B.S. and D.C. analyzed the data together with the other authors; A.P., B.D., G.Mi., D.D., F.B., V.P., G.Ma., B.S., and K.S. critically contributed to discussion; D.C. conceptualized all studies and supervised the work;

A.C-J. and D.C. wrote the manuscript; all authors edited and approved the final version of the manuscript.

Declaration of interest

The authors report no conflicts of interest relevant to this article.

Figure legends

Figure 1. Acute and chronic central TGR5 agonism counteracts obesity.

(A-B) Plasma and hypothalamic levels of total as well as specific BA species in chow lean and DIO mice. BA quantification was carried out after 2h re-exposure to food following a 24h fast. n of mice: **(A)** 8-9/group; **(B)** 4-9/group.

(C) Correlation between plasma and hypothalamic DCA levels. n=17 mice.

(C) mRNA expression of BA transporters OSTα, Ntcp and BSEP and of TGR5 in the hypothalamus of 24 fasted or 2h re-fed chow lean and DIO mice. n of mice: 5-6/group (chow); 7/group (DIO).

(E-H) Effect of an acute icv infusion of the selective TGR5 agonist CCDC (2.5 or 5µg) **(E-F)** or a BA mix (5µg) **(G-H)** on 24-h food intake (E and G) and body weight (BW) (F and H) in DIO mice. Animals were fasted for 24-h before icv treatment and subsequent exposure to food. n of mice: **(A-B)** 6-9/group; **(C-D)** 10-12/group.

(I-N) Effects of chronic icv infusion of CCDC (5µg/day) or its vehicle on daily BW **(I)**, body composition **(J-K)**, food intake **(L)**, blood glucose levels during an insulin tolerance test **(M)** and feed efficiency **(N)** in DIO mice. **(L)** was calculated from the start of the icv treatment; **(J-K)** were calculated from values obtained one day before the end of the study. n=6-7 mice/group; **(M)** insulin tolerance test carried out at the end of the chronic icv treatment. n=9-16 mice/group.

(O-R) Effect of chronic icv CCDC (5µg/day) or its vehicle administration in chow-fed ob/ob mice on BW **(O)**, cumulative food intake **(P)**, fat mass **(Q)** and lean mass **(R)**. n=9 mice/group.

Data are mean ± SEM. A repeated measures two-way ANOVA (E, G, I, M, O) and a one-way ANOVA (F), were carried out, followed by a Fisher's LSD test. For (A, B, D, H, J-L, N, P-R), unpaired t-tests or Mann-Whitney *U* test were carried out. In (D), unpaired t-tests were performed using ΔCT values; data are fold change from respective fasted group. *p<0.05, **p<0.01, ***p<0.001. See also Figure S1 and Table S1.

Figure 2. Chronic central TGR5 agonism increases energy expenditure by engaging the sympathetic nervous system.

(A) Energy expenditure (kcal/h) at normal housing temperature (22°C) and at thermoneutrality (30°C) during chronic icv infusion of CCDC or its vehicle. DIO mice were placed in calorimetric cages 8 days after micro-osmotic pump implantation. Grey areas indicate the night period; data are shown per hour. n=6 mice/ group.

(B) Effect of chronic icv infusion of CCDC or its vehicle on respiratory exchange ratio (RER) of mice in (A) during the night and the day period at 22°C. n=6 mice/group.

(C) Effect of chronic icv infusion of CCDC or its vehicle on locomotor activity of mice in (A) during the night and the day period at 22°C. n=6 mice/group.

(D-G) mRNA expression of lipolysis and thermogenesis markers in the WAT and BAT from chronic CCDC- and vehicle- treated DIO mice at 22°C (**D-E**), and 30°C (**F-G**). For **(F-G)**, mice were killed after 6 days at 30°C. n of mice: **(D)** 5-7/group; **(E)** 6-7/group; **(F)** 9-12/group; **(G)** 10-12/group.

(H-K) Effects of chemical sympathectomy with 6-OH-DOPA, followed by chronic icv infusion of CCDC (5µg/day) or its vehicle on BW **(H)**, body composition **(I-J)** and food

intake **(K)** in DIO mice. 6-OH-DOPA was injected i.p. (80mg/kg) during 3 consecutive days and animals were allowed to recover 1 week before the chronic icv treatment. n=9 mice/group.

Data are means ± SEM. For (A, B, C, H), a repeated measures two-way ANOVA was conducted followed by a Fisher's LSD test. For (D-G), unpaired t-tests were performed using ΔCT values; data are fold change from the vehicle group. For (I-K), unpaired t-tests were used. *$p<0.05$, **$p<0.01$, ***$p<0.001$; #$p<0.05$ treatment effect. See also Figure S2 and Table S1.

Figure 3. Knockdown of TGR5 in the mediobasal hypothalamus favors obesity.

(A-E) BW **(A)**, body composition **(B-C)**, food intake **(D)** and feed efficiency **(E)** following bilateral AAV-Cag-GFP control injection or AAV-Cag-Cre-GFP mediated knockdown of TGR5 in the MBH in TGR5$^{f/f}$ or C57BL/6J mice. Animals were on chow and then switched to a HFD (arrow). n=6-8 mice/group.

(F-J) BW **(F)**, body composition **(G-H)**, food intake **(I)** and feed efficiency **(J)** of already DIO TGR5$^{f/f}$ mice following bilateral AAV-Cag-GFP control injection or AAV-Cag-Cre-GFP mediated knockdown of TGR5 in the MBH. n=9-10 mice/group.

(K-M) Protein quantification of UCP-1 in the BAT (**K**) and of pHSL in the WAT (**L**) following 4h of cold exposure of HFD-fed TGR5$^{f/f}$ mice with (Cre) or without (GFP) MBH knockdown of TGR5. Representative blots per each tissue are depicted to the right of each histogram. mRNA expression of genes **(M)** related to thermogenesis, fatty acid use and glucose clearance in the WAT of 4h cold-exposed HFD-fed TGR5$^{f/f}$ mice with or without MBH knockdown of TGR5. n=6-7 mice/group.

(N-R) BW **(N)**, body composition **(O-P)**, food intake **(Q)** and feed efficiency **(R)** in TGR5$^{f/f}$-AAV-Cag-Cre-GFP and control mice switched to HFD and maintained at thermoneutrality (30°C). n of mice: **(N-P)** 10/group in; **(Q-R)** 9-10/group.

(S) mRNA expression levels of different neuropeptides, receptors, enzymes and neurotransmitter markers in FACS-sorted cells expressing or not TGR5. n=4 mice/group.

(T) Representative images of combined fluorescent *in situ* hybridization with immunohistochemistry showing that some Cre-GFP positive cells in the MBH express GAD65 (GABAergic neurons; left) and vGlut2 (glutamatergic neurons; right). Inserts show magnification of cells that co-express GFP and GAD65 or vGlut2 (yellow arrowheads), cells that only express GFP (green arrowheads) and cells that only express GAD65 or vGlut2, respectively (red arrowheads). Cells' nuclei were stained with DAPI. Scale bars= 100µm; 10µm for the inserts.

Data are means ± SEM. A repeated measures two-way ANOVA (A, F, N) and a one-way ANOVA (B-E) were used, followed by a Fisher's LSD test. In (G-L) and (O-R), unpaired t-tests were used. In (M), unpaired t-tests were performed using ΔCT values; data are fold change from the control group. For (S), no statistical analysis performed due to the low n of samples. *$p<0.05$, **$p<0.01$. See also Figures S3, S4 and Table S1.

Figure 4. Hypothalamic TGR5 contributes to the anti-obesity action of dietary BA supplementation.

(**A**) BW of TGR5$^{f/f}$ mice with (Cre) or without (GFP) hypothalamic knockdown of TGR5 exposed to either a HFD (black and red lines in A) or to a HFD enriched with 0.5% cholic acid (CA, grey and orange lines in A). (**B-E**) Magnitude of the effect of CA supplementation on BW loss (**B**), fat mass loss (**C**), food intake (**D**) and feed efficiency decrease (**E**) in TGR5$^{f/f}$ mice with (Cre) or without (GFP) hypothalamic knockdown of TGR5. n=8-10 mice/group.

Data are means ± SEM. For (A), a repeated measures three-way ANOVA (A) and unpaired t-tests (B-E) were used. In (B-E), for each genotype (GFP or Cre), data are expressed as fold change relative to the HFD control group. $^{***}p<0.001$; $^{###}p<0.001$ effect of TGR5 knockdown. See also Figure S5 and Table S1.

STAR Methods

1. LEAD CONTACT AND MATERIAL AVAILABILITY

Further information and requests for resources and reagents should be directed to and will be fulfilled by the Lead Contact, Daniela Cota (daniela.cota@inserm.fr). All main resources and reagents are listed in the Key Resources Table.

Materials Availability Statement

AAV-Cag-GFP and AAV-Cag-Cre-GFP correspond to virus n°1 and n°4 from our lab stock, respectively, and are available upon request.

2. EXPERIMENTAL MODEL AND SUBJECT DETAILS

All procedures involving live animals were approved and carried out in accordance with the National and European Directives 2013/63/EU, the French Ministry of Agriculture and Fisheries and the Ethical Committee of the University of Bordeaux and of the University of Lille for Animal Experimentation (authorizations #3959, #13394, #13395 and APAFIS#2617-2015110517317420 v5). Maximal efforts were made to avoid or reduce any suffering as well as to reduce the number of animals used.

Animals

Male C57BL/6J (Janvier, France) and TGR5$^{f/f}$ mice on a C57BL/6J background and generated as described in (Thomas et al., 2009) were used starting at 7-weeks-old (23g on average). In related studies we also used male ob/ob (B6.Cg-*Lep*^{ob}/J; Charles River, France), vGlut2-ires-Cre (Slc17a6tm2(cre)Lowl/J, JAX stock # 016963), vGat-

ires-Cre (B6J.129S6(FVB)-Slc32a1tm2(cre)Lowl/MwarJ, JAX stock # 028862) and TGR5-Tdt reporter (B6-Gpbar1^{tm1Ciphe}) mice. Reporter mice for TGR5 expression were generated by classical ES cell technology at Ciphe (Marseille-Luminy, France). Briefly an Haemagglutin (HA) Tag was inserted 3' in frame with the unique TGR5 exon after stop codon removal in order to generate a tagged TGR5 protein and a tandem Tomato (Tdt) Tag was inserted downstream an IRES sequence in order to use Tdt expression as a surrogate marker for TGR5 expression (see Figure S3F). HA and TdT expression was detected by qPCR in whole liver from reporter but not from control mice.

Animals were single housed in standard plastic rodent cages under a 12:12 h reversed light/dark cycle (lights on at 2:00 h) at 22 ± 2°C. Cages and enrichment (cellulose nestlets, wooden sticks and cardboard tunnels) were changed fortnightly. Mice received a standard chow diet (Standard Rodent Diet A03, SAFE, France; 3.236 kcal/g; 13.5% calories from lipids, 25.2% calories from proteins and 61.3% calories from carbohydrates) and water *ad libitum*, unless otherwise stated. For the diet-induced obesity model, mice were switched to a commercial high-fat diet (HFD) (D12492, Research Diets Inc. New Brunswick, NJ, USA; 5.24 kcal/g; 20% calories from proteins, 20% calories from carbohydrates, 60% calories from lipids) one week after arriving to the housing facility and were maintained on the diet for 12 weeks before the start of experiments until reaching 40g on average. A commercial HFD enriched with 0.5% cholic acid (D07033001, Research Diets Inc. New Brunswick, NJ, USA; 5.22 kcal/g; 20% calories from proteins, 20% calories from carbohydrates, 60% calories from lipids) that was matched to the HFD was used for studies on BA supplementation. Body weight was recorded weekly from all mice throughout the studies and daily when a particular experimental procedure was carried out. Food intake was recorded when a particular experimental procedure was carried out, and is indicated below. The feed

efficiency was calculated by dividing the body weight gain of a given time period into the total caloric intake during this same time. Animals that crumbled their food made it impossible to quantify their intake and were therefore excluded from the food intake and feed efficiency analyses.

At the end of the *in vivo* experiments, mice were killed to obtain either fresh or perfused tissues, as mentioned per procedure.

For obtaining perfused brain tissue, mice were deeply anesthetized with an i.p. injection of sodium pentobarbital (300 µl/30g Exagon® mixed with 30 mg/kg lidocaine) and perfused transcardially with ice-cold PBS (pH 7.4), followed by 4% paraformaldehyde (PFA, Sigma-Aldrich, France). Whole brains were extracted and post-fixed in 4% PFA overnight at 4°C, then cryo-protected with a 30% sucrose solution in PBS at 4°C and frozen. Coronal sections (30µm) were cut with a cryostat (CM1950, Leica, Germany), collected, and stored in an antifreeze solution (30% ethylene glycol, 30% glycerol in KPBS) at -20°C until analysis.

For fresh tissue sampling, mice were killed by decapitation (for plasma collection) or dislocation, and tissues collected, frozen on isopentane chilled on dry ice, and stored at -80°C until needed for molecular and biochemical analysis.

All animals were used in scientific experiments for the first time. This includes no previous exposures to pharmacological substances. Number of animals used in each experiment is indicated in the figure legends and in the statistical Table S1. Mice were allocated to experimental groups taking care to have similar body weight and fat mass content per group before the start of the experiments.

3. METHOD DETAILS

Body composition

Body composition analysis was performed *in vivo* by nuclear echo magnetic resonance imaging whole-body composition analysis (EchoMRI™ 900; EchoMedical Systems, Houston, TX, USA), as described previously (Cardinal et al., 2014). Analysis was performed at arrival to the housing facility, after the 12-week exposure to the HFD, and during chronic experiments, as indicated below. Briefly, mice were weighed and placed in the EchoMRI™ using a movement restrainer to allow proper measurements. All measures were taken in duplicates at the same time of day under free-feeding conditions. Data for fat and lean mass were extracted for analysis.

Surgeries

Mice were anesthetized using isofluorane 5% to induce the anesthesia and 1-2% during the surgery. Subcutaneous buprenorphine (0.1 mg/kg) and lidocaine at the level of the skull (0.1mL at 0.5%) were injected prior to surgery to reduce discomfort. Unconscious mice were placed on a stereotactic frame (David Kopf Instruments, USA); heat pads were used throughout the duration of the surgery to keep the body temperature stable. Eye ointment was applied to keep the eyes from drying. An incision was made to the skin to expose the skull after fur removal and asepsis with an iodine solution (Betadine®). For acute icv cannula placement, a burr hole for the stainless steel guide cannula (C313GS-5/SPC, G22; Plastics One®) was drilled on the skull (AP: -0.5; ML: -1.2; DV: -2.1). For chronic icv cannula placement, the same procedure as described above was used (AP: -0.3; ML: -1.0; DV: -2.5), with the addition of the subcutaneous implantation of a micro-osmotic pump (Alzet® System, model 1004;

pump rate 0.1µl/h during 28 days), which were connected to the icv cannula through a catheter. For the acute intra-hypothalamic cannula placement, a bilateral stainless steel cannula (C235I-SPC, G33; Plastics One®) targeting the mediobasal hypothalamus was implanted (AP: -1.1; ML: ±0.4; DV: -4.9). All cannulae were fixed to the skull with stainless steel screws and dental cement (MajorRepair®). For bilateral viral injections, different viruses were used: AAV1/2-Cre-CAG-hrGFP (referred to here as AAV-Cag-Cre-GFP) or its control (AAV-Cag-GFP) (Hebert-Chatelain et al., 2016), ssAAV-2-hGFAP-mCherry_iCre-WPRE-hGHp(A) (identifier: v233; referred to here as AAV-GFAP-Cre-mCherry) or its control (identifier: v222; AAV-GFAP-mCherry), and pAAV-hSyn-DIO-mCherry (Addgene, USA, #50459-AAV8). A craniotomy was made targeting the mediobasal hypothalamus (AP: -1.5; ML: ±0.3; DV: -5.8) and a 10 mm stainless steel injector (Nanofil® NF33BL, World Precision Instruments, USA) linked to a 10µL Hamilton syringe was slowly lowered into the target region to inject 500µL virus per side at 100nL/min. The injector was held in place for 3 min after injection to allow correct viral diffusion. Following surgery, all mice received 0.3 mL of saline solution subcutaneously, and meloxicam (5 mg/kg) for 2 days. Animals continued to be housed individually and body weight was monitored daily during one week to assess recovery.

Animal models

1. For acute icv experiments, a BA mix (sodium salts of taurocholic, glycocholic, deoxycholic, and cholic acids, Sigma-Aldrich) was diluted in artificial cerebrospinal fluid (aCSF), while 3-(2-chlorophenyl)-N-(4-chlorophenyl)-N, 5-dimethylisoxazole-4-carboxamide (Abcam), commonly known as CCDC, was diluted in 100% dimethylsulfoxide (DMSO) and delivered at the dose of 2.5 µg or 5 µg in a volume of 2

μL at a rate of 4 μL/min. Vehicles for the BA mix or CCDC consisted of 100% aCSF or DMSO, respectively. All acute drug infusions were carried out in 24 h fasted diet-induced obese C57BL/6J mice and compounds were administered just before the dark phase. Body weight was measured before and after 24 h from the icv administration; food intake was measured after 1, 2, 4 and 24 h from the icv administration. Correct cannula placement was assessed *in vivo* by icv infusion of neuropeptide Y (NPY; Phoenix Pharmaceuticals Inc.) in free-fed mice, as described previously (Bellocchio et al., 2013). Mice that ate >0.5g after 2 h of injection were included in the study.

2. For acute intra-hypothalamic experiments, diet-induced obese C57BL/6J mice bilaterally received CCDC (2 μg) or its vehicle at a volume of 0.2μL per side and a rate of 0.6μL/min. Body weight and food intake were recorded as described above. Correct intra-hypothalamic cannula placement was confirmed by blue dye injection before killing and was used as a criterion for inclusion.

3. For chronic icv experiments, diet-induced obese C57BL/6J mice were implanted with micro-osmotic pumps that were filled with CCDC diluted in 60% DMSO and 40% aCSF (mean pumping rate: 0.09μL/h; mean fill volume: 91.9μL). The catheter linked to each pump was filled with enough volume of aCSF to allow 3 days of post-surgical recovery before the start of the CCDC infusion. The concentration of CCDC was calculated to allow the delivery of 5 μg CCDC over 24h (stock concentration of 2.33 μg/μL). A mix of 60% DMSO and 40% aCSF was used for vehicle-treated animals. Body weight and food intake were recorded daily for 4 weeks. Body composition was measured at the start, 1 week after micro-pump implantation and at the end of the chronic treatment. A separate group of mice receiving chronic CCDC treatment were placed in calorimetric cages at 22°C and then housed at thermoneutrality (30°C) during 6 days to evaluate energy expenditure under blunted sympathetic activity. Another

group of mice underwent an insulin tolerance test after 4 weeks of chronic CCDC treatment. Details concerning these procedures are provided further below.

4. A group of chow-fed ob/ob mice underwent chronic icv delivery of CCDC or its vehicle, as described above. Body weight and food intake were recorded daily for 4 weeks. Body composition was measured at the start and at the end of the chronic treatment.

5. Chemical sympathectomy was carried out in diet-induced obese C57BL/6J mice by injecting i.p. for 3 consecutive days 80mg/kg of 6-hydroxydopamine (6-OH-DOPA) diluted in saline solution with 0.1% ascorbic acid (prepared fresh each day), as in (Quarta et al., 2010). One group of mice was killed after 1 week of the i.p. injections in order to assess the downregulation of tyrosine hydroxylase (TH) as marker of SNS activity in adipose tissues. After 1 week of 6-OH-DOPA administration, another group of mice underwent stereotaxic surgery coupled with subcutaneous micro-pump implantation for chronic icv delivery of either vehicle or CCDC, as described earlier. Food intake and body weight were recorded daily for 4 weeks; body composition was measured at the start of the i.p. injections, 3 days after micro-pump implantation and at the end of the study.

6. For the targeted downregulation of TGR5 expression within the mediobasal hypothalamus, the AAV-Cag-Cre-GFP or its control were administered in the following $TGR5^{f/f}$ models: lean mice on chow switched to a HFD and killed at 22°C (Cre linked AAV: $1.41E^{9}$ vg/mL; control: $1.17E^{9}$ vg/mL); lean mice on chow switched to a HFD and maintained at 30°C during HFD exposure (Cre linked AAV: $1.41E^{9}$ vg/mL; control: $1.17E^{9}$ vg/mL); lean mice on chow switched to a HFD for 2 weeks and killed after an acute cold challenge consisting of 4h exposure at 4°C (Cre linked AAV: $1.41E^{11}$ vg/mL;

control: 1.17E^{9} vg/mL); diet-induced obese TGR5$^{f/f}$ mice (Cre linked AAV: 1.41E^{11} vg/mL; control: 1.17E^{9} vg/mL); and lean TGR5$^{f/f}$ mice on chow switched to a HFD or to a HFD enriched with 0.5% CA (Cre linked AAV: 1.41E^{9} vg/mL; control: 1.5E^{11} vg/mL). The AAV-GFAP-Cre-mCherry (5.2E^{12} vg/mL) or its control (6.0E^{12} vg/mL) were used for lean mice on chow switched to a HFD only. Viral localization within the mediobasal hypothalamus was assessed by neuroanatomical analysis. In all these models, food intake and body weight were recorded daily; body composition was measured at time of AAV injection and one day before killing.

7. For the targeted labelling of glutamatergic and GABAergic cells within the mediobasal hypothalamus, a pAAV-hSyn-DIO-mCherry (2.1E^{13} vg/mL) was administered in chow-fed vGlut2-ires-cre and vGat-ires-Cre*B6 mice. Animals were killed after 3 weeks from the surgery for subsequent cell laser capture microdissection on the mediobasal hypothalamus (see further below).

Pharmacokinetics of CCDC

The abundance of CCDC was measured after an acute icv administration of 5µg, and after 4 weeks of continuous icv infusion. Groups of 3 mice were killed by decapitation at 15, 30, 60, 120 and 240 min after the acute icv injection, and the hypothalamus and the rest of the brain were collected as fresh tissue. Blood samples after acute or 4 weeks icv CCDC administration were collected in heparin tubes, centrifuged at 5000 rpm for 10 min at 4°C, and plasma was collected and frozen at -80°C until analysis. Quantification was carried out by liquid-chromatography mass-spectrometry (LC-MS/MS).

Sample preparation

Plasma: Compound was extracted from plasma samples using a vortex, with an ice-cold acetonitrile/methanol (50:50) solution containing the internal standard, in a 1 to 10 ratio. After centrifugation (12000 rpm, 10 min, 4°C) of the homogenate samples, the supernatants were transferred into Matrix tubes for LC-MS/MS analysis.

The standard curve was generated using naïve mouse plasma (from vehicle animals), spiked with the appropriate compound solution resulting in 10 different concentrations of CCDC. This standard curve was then extracted as the plasma samples (in a 1 to 10 ratio) leading to concentration from 0.1 to 3000nM (0.1, 0.3, 1, 3, 10, 30, 100, 300, 1000 and 3000nM).

Hypothalamus: After 5 freeze-thaw cycles (4°C, 25min / -80°C, 25min), CCDC was extracted from hypothalamus in an acetonitrile/methanol (50:50) solution (9mL per gram of tissue) with 2 cycles of 10 minutes of sonication. After centrifugation (12000 rpm, 10 min, 4°C) of the homogenates, the supernatants were diluted in a 1 to 2 ratio with an ice-cold acetonitrile/methanol (50:50) solution containing the internal standard. Each tube was vigorously mixed, centrifuged (12000 rpm, 10 min, 4°C) then the supernatant was transferred into Matrix tubes for LC-MS/MS analysis.

Due to the small volume of hypothalamus homogenate available, the standard curve was generated using the appropriate CCDC solution (in acetonitrile/methanol), diluted in a 1 to 2 ratio with an ice-cold acetonitrile/methanol (50:50) solution containing the internal standard, leading to concentration from 0.1 to 3000nM (0.1, 0.3, 1, 3, 10, 30, 100, 300, 1000 and 3000nM). Two points at 30 and 100nM final were prepared in the hypothalamus homogenate and no matrix effect was observed.

Rest of the brain: After 13 freeze-thaw cycles (4°C, 30min/-196°C, 5min), the rest of the brain was homogenate in a water/methanol (50:50) solution (1mL per gram of

tissue) with 10 minutes of sonication. Then, after two more cycles of freeze-thaw (4°C, 30min / -196°C, 5min), the homogenates were extracted using an acetonitrile/methanol (50:50) solution (4mL per gram of tissue) with 2 cycles of 10 minutes of sonication. The samples were centrifuged (12000 rpm, 10 min, 4°C) then the supernatants were diluted in a 1 to 2 ratio with an ice-cold acetonitrile/methanol (50:50) solution containing the internal standard. Each tube was vigorously mixed, centrifuged (12000 rpm, 10 min, 4°C) and the supernatant transferred into Matrix tubes for LC-MS/MS analysis.

The standard curve was generated using naïve mouse brain (from vehicle animals), spiked with the appropriate compound solution resulting in 10 different concentrations of CCDC. This standard curve was then extracted as the brain samples (in a 1 to 2 ratio) leading to concentration from 0.1 to 3000nM (0.1, 0.3, 1, 3, 10, 30, 100, 300, 1000 and 3000nM).

LC-MS/MS

LC-MS/MS analysis was performed on an UPLC system Acquity I Class (Waters©), combined with a triple quadrupole mass spectrometer Xevo TQD (Waters©).

The column, placed at 40°C, was an Acquity BEH C18 50*2.1mm, 1.7µm column (Waters©) and the following mobile phases were used: 5mM ammonium formate pH 3.75 in water, as solvent (A) and 5 mM ammonium formate pH 3,75 in acetonitrile as solvent (B). At a flow rate of 600µL/min, the analytical method started at 98% (A) for 10s, then the percentage of B gradually increased at 98% until 2 min, hold at 98% (B) for 30s before returning to the initial conditions, hold 1.5 min. The samples were maintained at 10°C and the injection volume was 1µL.

MS analyses were performed under MRM detection using the following transitions: m/z 361.0 > 178.0 for CCDC with a cone voltage and a collision energy of 46 and 24V

respectively; and 260.2 > 116.1 for the internal standard (propranolol, 100nM) with a cone voltage and a collision energy of 40 and 18V respectively. Argon was used as collision gas. The capillary voltage was set at 0.5 kV. The source temperature was 150°C, desolvation temperature was 600°C, desolvation gas flow was 1200 L.h-1 and cone gas flow was 50 L.h-1. All data were acquired and processed using the MassLynx 4.0 software (Waters©).

Insulin tolerance test

After 4 weeks of chronic icv infusion with CCDC or its vehicle, diet-induced obese mice were fasted for 6 h and were injected i.p. with 0.5 U/kg of insulin (Umuline Rapide, Lilly, France). Blood samples were collected from the tail vein and glucose was measured using glucose strips (OneTouch, Vita, France) at baseline, 15, 30, 60, 90 and 120 min after the administration of insulin.

Indirect calorimetry

Indirect calorimetry, in-cage locomotor activity and gas exchange analysis were carried out in light, temperature and humidity controlled calorimetric chambers (TSE Systems GmbH, Bad Homburg, Germany), as in (Cardinal et al., 2014). Diet-induced obese mice receiving chronic icv infusion of CCDC or its vehicle were acclimated for 3 days in the chambers before recording. O_2 consumption and CO_2 production were measured every 20 min in order to calculate the gas exchange, the respiratory quotient and the energy expenditure. At the same time, in-cage locomotor activity was determined using a tridimensional infrared light beam system. Food intake was measured continuously

by integration of scales inside the cages. A meal consisted of the consumption of at least 0.03g of food separated from the next feeding episode by at least 10 min (Hassouna et al., 2012). Body weight was measured daily during this time and the temperature was fixed to 22°C. When recording at thermoneutrality, the temperature in the calorimetric chambers was increased to 30°C.

Food preference test

Naïve TGR5$^{f/f}$ lean mice were placed in individual cages and habituated to 2 food hoppers filled with chow and placed inside each cage for 5 days. During this time, mice were exposed to a small quantity of the HFD enriched with 0.5% CA to avoid neophobia during the behavioral experiment. On day 6, one food hopper was filled with the HFD supplemented with CA while the other continued to have chow. The hoppers with food were removed from the cage 1 h before the preference test, which was performed during the light phase. Mice were then allowed access to the two hoppers during 1 h. The hoppers were weighed before and after access to food.

BA quantification

BA quantification in plasma and hypothalamus of chow-fed lean and DIO mice.

For plasma and hypothalamic BA measurements, chow lean and DIO mice were killed by decapitation 2 hours after re-exposure to either chow or HFD following a 24h fast. Plasma was obtained as described above in (Pharmacokinetics of CCDC). The hypothalamus was collected and immediately frozen in isopentane chilled on dry ice. Samples were stored at -80°C until analysis. BA were analyzed using ultra-

performance liquid chromatography-tandem mass spectrometry (UPLCMS/MS) according to previous work (Tremaroli et al, 2015). Briefly, brain samples (20-30 mg wet weight) were homogenized and extracted in 500 µL of methanol containing deuterated internal standards (d4-TCA, d4-GCA, d4-GCDCA, d4-GUDCA, d4-GLCA, d4-UDCA, d4-CDCA, d4-LCA; 25 nM of each). After 10 min of homogenization/extraction using the TissueLyser II instrument (Qiagen, Sweden) and 10 min of centrifugation at 20 000 g, the supernatant was evaporated under a stream of nitrogen and reconstituted in 100 µL methanol:water [1:1]. The samples were injected (5 µL) and BA were separated on a Kinetex C18 column (1.7 µ, 2.1 x 100 mm; Phenomenex, USA) using water with 7.5 mM ammonium acetate and 0.019% formic acid (mobile phase A) and acetonitrile with 0.1% formic acid (mobile phase B). The chromatographic separation started with 1 minute isocratic separation at 20% B. The B-phase was then increased to 35% during 4 min. During the next 10 min the B-phase was increased to 100%. The B-phase was held at 100% for 3.5 min before returning to 20%. The total runtime was 20 min. BA were detected using multiple reaction monitoring (MRM) in negative mode on a QTRAP 5500 mass spectrometer (Sciex, Concord, Canada) and quantification was made using external standard curves.

Plasma BA quantification in pharmacological studies.

For measurements of circulating BA from chronic pharmacological studies, free-fed diet-induced obese mice were killed by decapitation after 10 days of chronic CCDC treatment. BA were precipitated from plasma and pellets solubilized in MeOH as described previously (Garcia-Canaveras et al., 2012). The separation of BA was carried out on a Symmetry C18 Luna column (250 mm × 2.1 mm, particle size 5 µm) from Phenomenex (Le Pecq, France). The oven temperature was set at 30°C. Solvent A was water containing 20 mM ammonium acetate, adjusted to pH 8 and solvent B

was acetonitrile. Solvents were delivered at a total flow rate of 500 µl/min^{-1}. After a 5 min plateau with 28% B, the gradient profile was from 28% B to 90% B linearly in 15 min, followed by a 2 min plateau with 90% B. Column re-equilibration was performed for 4 min. The injection cycle was 26 min. BA quantification was then performed by high-performance liquid chromatography (UFLC-XR device; Shimadzu, Kyoto, Japan) coupled to tandem mass spectrometry MS/MS (QTRAP 5500 hybrid system, equipped with a Turbo VTM ion source; AB Sciex, Foster City, CA, USA). Instrument control, data acquisition and processing were performed using the associated Analyst 1.5.2 software (AB Sciex, Concord, ON, Canada). The inter- and intra-day precisions of the BA concentration assay are <15%, except for HCA and LCA (<30%).

Single cells laser capture microdissection

Four vGlut2-ires-cre mice and 3 vGat-ires-Cre*B6 mice having received an pAAV-hSyn-DIO-mCherry in the mediobasal hypothalamus were used. Coronal sections of perfused brains (10 µm thickness) covering the region from -1.34 to -1.94 mm caudal to bregma, as defined by Paxinos and Franklin, were made using a CM3050 S cryostat (Leica, Wetzlar, Germany) and mounted on polyethyl-ene-naphthalate membrane 1mm glass slides (P.A.L.M. Microlaser Technologies AG, Bernried, Germany) that were pretreated to inactivate RNase. Subsequently, sections were dehydrated in a series of pre-cooled ethanol baths (40s in 95% and twice 40s in 100%) and air-dried. Laser microdissection of mCherry-expressing cells was performed using a PALM MicroBeam microdissection system version 4.6 equipped with the P.A.L.M. RoboSoftware (P.A.L.M. Microlaser Technologies AG, Bernried, Germany). Laser power and duration were adjusted to optimize capture efficiency. Microdissection was

performed at 63X magnification. A total between 800/900 cells per mice was captured. Cells were collected in adhesives caps and re-suspended in PK buffer (PK buffer from RNeasy FFPE KIt, Qiagen, Chatsworth, USA), and stored at −80°C until extraction was done. Total RNA was extracted from microdissected cells using the RNeasy® FFPE Kit (Qiagen, Hilden, Germany) according to the manufacturer's protocol. The integrity of the RNA was checked by capillary electrophoresis using the RNA 6000 Pico Labchip kit and the Bioanalyser 2100 (Agilent Technologies, Massy, France), and quantity was estimated by spectrophotometry using a Denovix DS-11 (Denovix, Wilmington, USA).

Isolation of hypothalamic TGR5-expressing cells using fluorescence-activated cell sorting (FACS)

The mediobasal hypothalamus of 4 TGR5-Tdt reporter and 4 wild-type, control mice was microdissected and enzymatically dissociated using a Papain Dissociation System (Worthington, Lakewood, NJ) to obtain a single-cell suspension. FACS was performed using an ARIA SORP cell sorter cytometer device (BD Bioscience, Inc). The sorting parameter were based on measurements of Tomato fluorescence (excitation 561nm; detection: bandpass 675+/-20nm) by comparing cell suspensions from TGR5-Tdt and control animals. For each animal, 40 to 110 tomato-positive and an equal amount of tomato-negative cells were sorted directly into 10 µl of lysis buffer (0.1% Triton® X-100 and 0.4unit/µl RNaseOUT™, Life Technologies).

Quantitative Real-Time PCR

qPCR on tissues

qPCR was carried out in hypothalamic samples (reference genes: Sdha and Tuba4a) from chow-fed and HFD-fed, diet-induced obese C57BL/6J mice, either fasted for 24h or re-exposed to food for 2h after the 24h fast. qPCR was also performed in epididymal white adipose tissue (WAT; reference genes: Gapdh and Ppia) and brown adipose tissue (BAT; reference genes: Sdha and Nono) from free-fed diet-induced obese mice receiving chronic CCDC treatment or vehicle killed by decapitation at 22°C; WAT and BAT from free-fed diet-induced obese mice receiving chronic CCDC treatment or vehicle and killed by decapitation at 30°C (reference genes: Ppia and Nono); WAT (reference genes: Sdha and Nono) from free-fed mice on a HFD that received AAV-Cag-Cre-GFP or its control and were killed by decapitation at 4°C; hypothalamus (reference genes Ppia and Rpl13a) from free-fed mice on a HFD that received the AAV-Cag-Cre-GFP or its control and were killed by perfusion at 22°C; and hypothalamus (reference genes: Sdha, Eef1a1 and Ywha2) from free-fed mice on a HFD that received the AAV-GFAP-Cre-mCherry or its control and were killed by perfusion at 22°C.

For samples from hypothalamic TGR5 deletion models, 10 punches of 2 mm (cut from the 30 µm slices) containing the mediobasal hypothalamus, as well as the cortex, amygdala and ventral tegmental are (VTA), were obtained per animal, placed on 100µL proteinase K digest buffer (Qiagen) and frozen at 80°C until qPCR analysis.

Samples were homogenized in Tri-reagent (Euromedex, France). RNA from fresh tissue was isolated using a standard chloroform/isopropanol protocol, while RNA from perfused samples was isolated using Quick-RNA™ FFPE Kit (ZYMO Research). cDNA was synthesized from 2 µg of total RNA using Maxima Reverse Transcriptase (Fisher Scientific) and primed with oligo-dT primers (Fisher Scientific) and random primers (Fisher Scientific). qPCR was performed using a LightCycler® 480 Real-Time PCR

System (Roche, Meylan, France). qPCR reactions were done in duplicate for each sample (except on hypothalamic samples from mice receiving the AAV-GFAP-Cre-mCherry or its control, which were run in triplicates), using transcript-specific primers, cDNA (4 ng) and LightCycler 480 SYBR Green I Master (Roche) in a final volume of 10 µL. Primer sequences are reported in Table S3. Relative expression analysis was normalized against two reference genes (except on hypothalamic samples from mice receiving the AAV-GFAP-Cre-mCherry or its control, which were normalized to three reference genes), depending on the tissue (see above). The relative level of expression was calculated using the comparative 2-ΔΔCT method. mRNA expression levels are expressed as the fold change from the reference group (as mentioned in the figure legends) after normalization.

mRNA from liver samples of TGR5-Tdt reporter and control mice were extracted after shredding liver lobes in Trizol, phenol-chloroform extraction and precipitation by isopropanol was used. qPCR was performed as in…….to assess expression of both HA-tag and Tandem Tomato. Primer sequences are reported in Table S3. Cyclophilin A was used as reference gene.

qPCR on laser capture microdissected cells

cDNA was generated using the qScript XLT cDNA SuperMix (Quanta Biosciences) following the manufacturer's instructions. qPCR was performed as described above. Primer sequences are reported in Table S3. The glyceraldehyde-3-phosphate dehydrogenase (Gapdh) and Elongation factor 1-alpha 1 (Eef1a1) were used as reference genes.

qPCR on FACS-sorted cells

Total RNA obtained from FACS-sorted tomato-positive cells was reverse transcribed using High capacity cDNA Reverse transcription kit (Applied Biosystems™, # 4368814) after a DNAse treatment (DNase I, Amplification Grade, Invitrogen™, #18068015). A linear preamplification step was performed using the TaqMan® PreAmp Master Mix Kit protocol (Applied Biosystems™, # 4488593). Next, a real-time PCR was carried out on Applied Biosystems 7900HT Fast Real-Time PCR System using the TaqMan® probes (see Table S3) and TaqMan™ Universal Master Mix II (Applied Biosystems™, # 4440049). Control housekeeping genes r18S and actin were used for analysis. Gene expression data were analyzed using the $2^{-\Delta\Delta Ct}$ method between negative and positive tomato FACS-sorted cells.

Western blot analysis

WAT and BAT samples from free-fed sympathectomized mice, as well as from free-fed TGR5$^{f/f}$ mice receiving the AAV-Cag-Cre-GFP or its control and sacrificed at 4°C were obtained after killing by decapitation.

Samples were homogenized in radioimmunoprecipitation assay buffer with phosphatase and protease inhibitors (Santa Cruz Biotechnology) for obtaining protein extracts. Proteins were separated in an SDS-polyacrylamide gel (9-13%) by electrophoresis and transferred to nitrocellulose membranes, which were then blocked for 1h with 5% skim milk powder and incubated overnight at 4°C with the following primary antibodies: hormone-sensitive lipase (HSL, 1:1000, #4107, Cell Signaling), phospho-HSL ser563 (1:1000, #4139, Cell Signaling), uncoupling protein-1 (UCP-1, 1:1000, #10983, Abcam), tyrosine hydroxylase (TH, 1:1000, #152, Millipore), and β-actin (1:2000, #4967, Cell Signaling), which was used as loading control. After washing

in Tris-buffered saline with 0.05% Tween (TBST), the membranes were incubated for 1 h at room temperature with secondary antibody conjugated with horseradish peroxidase (goat anti-rabbit; 1:2000; Cell Signaling Technology). After 3 washes in TBST, immunoreactive bands were visualized using enhanced chemiluminescence (ECL Plus, PerkinElmer) then exposed on a ChemiDoc® MP Imaging System (Biorad). Bands were quantified using ImageJ software (NIH, Bethesda, MA). When necessary, membranes were stripped after protein detection for 10 min at 55°C with a solution containing 62.5 mmol/l Tris-HCl, 100 mmol/l 2-mercaptoethanol, and 2% SDS, blocked, and reblotted with another primary antibody.

Assessment of Cre recombination by PCR

Perfused brain slices containing the mediobasal hypothalamus from TGR5$^{f/f}$ receiving the AAV-Cag-Cre-GFP or its control, or the AAV-GFAP-Cre-mCherry or its control were genotyped by PCR to evaluate recombination in genomic DNA. Tissue from naïve C57BL/6J mice (wild type, WT) was used as a negative control, whilst tissues from whole body TGR5 knockout obtained by crossing TGR5$^{f/f}$ with CMV-Cre mouse strain (Schwenk et al., 1995) (referred as +/ex) was used as a positive control of excision. Five perfused brain slices per animal were incubated overnight at 56°C in Proteinase K buffer (100 mM Tris-HCl pH8, 5 mM EDTA, 0.2 % SDS, 200 mM NaCl, 0,2 mg/mL PK); after 10 min at 13200 rpm, the supernatants were purified by vacuum on silica columns, according to the manufacturer's protocol (Macherey-Nagel kit), on a Zephyr automatic workstation (Perkin-Elmer). PCR assay was carried out on a Bio-Rad C1000 thermal cycler, in a 20 µL volume, using GoTaq G2 Hot Start Green Master Mix

(Promega), and 0.2 µM of each primer. PCR products were analyzed on a Labchip GX microfluidic electrophoresis system (Perkin-Elmer) using the DNA5k kit.

Neuroanatomical analysis

Perfused brain slices from TGR5$^{f/f}$ mice receiving the AAV-Cag-Cre-GFP or its control, or the AAV-GFAP-Cre-mCherry or its control were analyzed.

Immunohistochemistry

All immunofluorescence steps were performed under gentle agitation at room temperature. Slices were rinsed three times in PBS for 10 min and then incubated with primary antiserum overnight. Primary antibodies were diluted in PBS containing 0.3% Triton X-100 (PBST) and 5% normal serum (goat or donkey depending on the specie used to generate the secondary antibodies) except when Mouse on Mouse Fluorescein kit was used. After incubation, slices were washed again three times in PBS for 10 min and incubated in secondary antibody solution for 2 h in the dark. Secondary antibodies were diluted in PBS containing 0.3% Triton X-100 except when Mouse on Mouse Fluorescein kit was used. After a 5 min rinse in PBS, slices were incubated 5 min with the nuclear marker 4',6'-diamidino-2-phenylindol (DAPI; 1:10000; # D1306, Molecular Probes). After a final rinse in PBS, slices were mounted on gelatin coated slides and coverslipped using Prolong gold anti-fade (# P36930, Vector Laboratories) and then stored at 4°C until use.

For visualization of microglia and neurons, we used a double immunohistofluorescent technique. Slices were incubated in a chicken antiserum against NeuN (1:500, #ABN91, Millipore) and in a rabbit antiserum against Iba-1 (1:2000, #019-19741,

Wako). Slices were then incubated in a donkey anti-chicken secondary antibody conjugated to Alexa 647 (#703-606-155, Jackson ImmunoResearch Labs) and in a donkey anti-rabbit secondary antibody conjugated to Alexa 448 (#711-545-152, Jackson ImmunoResearch Labs) or to Alexa 594 (#711-585-152, Jackson ImmunoResearch Labs) for TGR5$^{f/f}$-AAV-GFAP-Cre-mCherry/TGR5$^{f/f}$-AAV-GFAP-mCherry and TGR5$^{f/f}$-AAV-Cag-Cre-GFP/TGR5$^{f/f}$-AAV-Cag-GFP mice respectively, all diluted 1:2000.

For visualization of astrocytes, we used a double immunohistofluorescent technique. We used a rabbit antiserum against GFAP (1:1000, #Z0334, Agilent) and a monoclonal mouse antibody against protein S100β-subunit (S100β, 1:10000, clone SH-B1, #S2532, Sigma-Aldrich). Slices obtained from TGR5$^{f/f}$-AAV-Cag-Cre-GFP/TGR5$^{f/f}$-AAV-Cag-GFP mice, after the initial PBS rinses, were incubated 30 min in 3%H_2O_2 PBST and rinsed three times in PBS for 5 min. After incubation in the primary antibodies, species-specific secondary antibodies which have been raised in goat [anti-rabbit conjugated to Alexa 555 (#4413, Cell Signaling) and anti-mouse conjugated to peroxidase (#AP124P, Millipore) both diluted 1:500] were used. After rinses in wash buffer (prepared according to the manufacturer's protocol), slices were incubated for 10 min in TSA plus Cy5 system (1:300 in amplification buffer provided by the manufacturer, #FP1117, Perkin Elmer). Slices obtained from TGR5$^{f/f}$-AAV-GFAP-Cre-mCherry/TGR5$^{f/f}$-AAV-GFAP-mCherry mice were incubated in the rabbit antiserum against GFAP and then in a goat anti-rabbit secondary antibody conjugated to Alexa 647 (1:500, #4414, Cell Signaling). Then slices were treated according to the manufacturer's instructions of the Mouse on Mouse Fluorescein kit (#FMK-2201, Vector Laboratories) to reveal the S100β staining. Briefly, slices were incubated in an Avidin/Biotin blocking kit (#SP-2001, Vector Laboratoires), 1h in a proprietary Mouse

IgG blocking reagent, 30 min in the monoclonal mouse antibody against S100β (see above, 1:1000 in the manufacturer's diluent), 10 min in a mouse on mouse (M.O.M.™, Vector) Biotinylated Anti-Mouse Ig Reagent and 5 min in a cell sorter grade of Fluorescein Avidin D.

Images were acquired on a Leica DM6 CFS TCS SP8 confocal microscope using an objective 10X (voxel size: 1.0823x1.0823x4.2839 μm^3) or an objective 40X (voxel size: 0.2705x0.2705x0.3462μm^3). Laser diodes used were at 405 nm (DAPI), 488 nm (Alexa 488 or Flurorescein or GFP), 552 nm (Alexa 555 or mCherry) and 638 nm (Alexa 647 or Cy5). Parameters were determined at the beginning of the acquisition and were maintained for all acquisitions of the same experiment. All presented images are Z projection (maximal intensity) of a given stack.

Fluorescent in situ hybridization combined with immunohistochemistry

Perfused brain slices from 5 $TGR5^{f/f}$ mice receiving the AAV-Cag-Cre-GFP were used. Digoxigenin-labeled riboprobe against the glutamatergic marker vesicular glutamate transporter 2 (vGlut2) and the GABAergic marker GABA synthesizing enzyme GAD65 were obtained as previously described (Saucisse et al., 2020). Free-floating sections were treated with 0.2M HCl then acetylated with 0.25% acetic anhydride in 0.1 M triethanolamine, pH=8.0 for 10 min. Between all steps, sections were rinsed in PBS with 0.01% diethylpyrocarbonate. VGlut2-DIG or GAD65-DIG was dissolved 1/1000 in hybmix solution (50% deionized formamide, 20mM Tris at pH=8.0, 300mM NaCl, 5mM EDTA, 10% dextran sulfate, 1X Denhardt's solution, 0.5mg/mL tRNA, 0.2mg/mL acid-cleaved carrier DNA from salmon's sperm, 1M DTT dissolved in water containing 0.01% DEPC) and linearized by heating at 90°C for 5 min. After hybridization overnight at 70°C, sections were washed at 70°C with increased stringency buffers (5X saline

sodium citrate (SSC) for 5min, 2X SSC + 50% Formamide amide, 1X SSC + 50% Formamide amide and 0.1X SSC for 30min each, with 0.1% Tween20 added to each buffer). Sections were incubated 30 min in 3% H_2O_2 in TNT (100mM Tris-HCl, 150mM NaCl, 0.05% Tween20) to quench endogenous peroxydases, 20 min in 0.2M HCl, 1h in blocking buffer (#FP1012; Akoya Biosciences), 2h in antidigoxigenin-POD antibody (1:1500 in the blocking buffer; #11207733910; Roche), 30 min in TSA plus Cy3 system (1:100 in 1X Plus amplification buffer provided by the manufacturer; #NEL744001KT; Akoya Biosciences), 30 min in 3% H_2O_2 TNT to block HRP and overnight at 4°C in goat anti-GFP antibody (1/:400 in PBST; #AB0066-200; Sicgen). Between all steps, sections were rinsed in TNT. After 3 washes in PBS, slices were incubated 2h in a donkey anti-goat secondary antibody conjugated to Alexa 488 (1:500 in PBST; #A11055; Life technologies). After 3 washes in PBS, slices were stained for 5 min with DAPI (1:20 000, in PBS), washed in 50mM Tris (pH=7.5), mounted on gelatinized slides, cover-slipped using Prolong® and kept at 4°C until use. All steps were carried out at room temperature unless stated otherwise.

Confocal images of the medio-basal hypothalamus were collected using a Leica DMi6000 TCS SP8 X confocal microscope (Leica microsystems, Germany) enabled with a 20X/NA 0.75 oil immersion objective (Leica HC PL APO CS2), a laser diode at 405nm (DAPI), a white light excitation laser (set at 499nm for AF488 and at 553nm for Cy3) and hybrid detectors. Images were corrected automatically for brightness and contrast, and analyzed using ImageJ (National Institutes of Health, USA). For each image, we used the plugin Cell counter in ImageJ to select and count GFP positive cells that co-expressed (or not) vGlut2 or GAD65. The analysis was made on 2-8 medio-basal hypothalami from 2-4 sections per animal. For illustration purpose, some images were also taken with a 63X/NA 1.4 oil objective.

4. QUANTIFICATION AND STATISTICAL ANALYSIS

Statistical analysis was carried out using the GraphPad Prism Software version 8.0 for Windows (La Jolla, CA, USA). Data are expressed as mean ± S.E.M. Sample sizes for experiments were determined based on sample sizes used in similar experiments reported previously in the literature.

The statistical test used for each comparison is described in the figure legends corresponding to the specific figure and further detailed in table S1. Briefly, when comparing 2 groups, data were analyzed by an unpaired Student's t-test (Shapiro-Wilk test for normality when small sample sizes, otherwise, Kolmogorov-Smirnov test for normality), or a Mann-Whitney U test (nonparametric). When comparing 3 or more groups, data were analyzed by one-way ANOVA. Two-way ANOVAs were performed for analyzing body weight, body composition, cumulative food intake and feed efficiency considering genotype (with or without hypothalamic deletion of TGR5) and diet (HFD or HFD+CA) as factors. Body weight, insulin tolerance test, food intake, energy expenditure, RER, meal size, and locomotor activity over time were analyzed by two-way repeated measures ANOVA considering treatment and time as factors. For analyzing energy expenditure at 22°C or at 30°C, a three-way ANOVA was carried out considering time of day (day or night), treatment (Vehicle or CCDC) and temperature (22°C or 30°C) as factors. Similarly, a three-way ANOVA was carried out for analyzing body weight and food intake over time on $TGR5^{f/f}$ mice receiving AAV-Cag-Cre-GFP or its control that were either exposed to a HFD or a HFD+CA, considering time, genotype and diet as factors. Fisher's LSD post-hoc tests were run when applicable

for identifying differences amongst groups. In all cases, tests were considered significant when $p<0.05$.

5. DATA AND CODE AVAILABILITY

This study did not generate any unique datasets or code.

6. ADDITIONAL RESOURCES

None.

Supplemental information

Supplemental information includes 3 tables and 5 figures.

References

Bellocchio, L., Soria-Gomez, E., Quarta, C., Metna-Laurent, M., Cardinal, P., Binder, E., Cannich, A., Delamarre, A., Haring, M., Martin-Fontecha, M., Vega, D., Leste-Lasserre, T., Bartsch, D., Monory, K., Lutz, B., Chaouloff, F., Pagotto, U., Guzman, M., Cota, D., and Marsicano, G. (2013). Activation of the sympathetic nervous system mediates hypophagic and anxiety-like effects of CB(1) receptor blockade. Proc Natl Acad Sci U S A *110*, 4786-4791.

Blaszkiewicz, M., and Townsend, K.L. (2016). Adipose Tissue and Energy Expenditure: Central and Peripheral Neural Activation Pathways. Curr Obes Rep *5*, 241-250.

Broeders, E.P., Nascimento, E.B., Havekes, B., Brans, B., Roumans, K.H., Tailleux, A., Schaart, G., Kouach, M., Charton, J., Deprez, B., Bouvy, N.D., Mottaghy, F., Staels, B., van Marken Lichtenbelt, W.D., and Schrauwen, P. (2015). The Bile Acid Chenodeoxycholic Acid Increases Human Brown Adipose Tissue Activity. Cell Metab *22*, 418-426.

Cardinal, P., Andre, C., Quarta, C., Bellocchio, L., Clark, S., Elie, M., Leste-Lasserre, T., Maitre, M., Gonzales, D., Cannich, A., Pagotto, U., Marsicano, G., and Cota, D.

(2014). CB1 cannabinoid receptor in SF1-expressing neurons of the ventromedial hypothalamus determines metabolic responses to diet and leptin. Mol Metab *3*, 705-716.

Clapham, J.C. (2012). Central control of thermogenesis. Neuropharmacology *63*, 111-123.

Dietrich, M.O., and Horvath, T.L. (2013). Hypothalamic control of energy balance: insights into the role of synaptic plasticity. Trends Neurosci *36*, 65-73.

Doignon, I., Julien, B., Serriere-Lanneau, V., Garcin, I., Alonso, G., Nicou, A., Monnet, F., Gigou, M., Humbert, L., Rainteau, D., Azoulay, D., Castaing, D., Gillon, M.C., Samuel, D., Duclos-Vallee, J.C., and Tordjmann, T. (2011). Immediate neuroendocrine signaling after partial hepatectomy through acute portal hyperpressure and cholestasis. J Hepatol *54*, 481-488.

Evans, K.A., Budzik, B.W., Ross, S.A., Wisnoski, D.D., Jin, J., Rivero, R.A., Vimal, M., Szewczyk, G.R., Jayawickreme, C., Moncol, D.L., Rimele, T.J., Armour, S.L., Weaver, S.P., Griffin, R.J., Tadepalli, S.M., Jeune, M.R., Shearer, T.W., Chen, Z.B., Chen, L., Anderson, D.L., Becherer, J.D., De Los Frailes, M., and Colilla, F.J. (2009). Discovery of 3-aryl-4-isoxazolecarboxamides as TGR5 receptor agonists. J Med Chem *52*, 7962-7965.

García-Cáceres, C., Balland, E., Prevot, V., Luquet, S., Woods, S.C., Koch, M., Horvath, T.L., Yi, C.X., Chowen, J.A., Verkhratsky, A., Araque, A., Bechmann, I., Tschöp, M.H. (2019). Role of astrocytes, microglia, and tanycytes in brain control of systemic metabolism. Nat Neurosci *22*, 7-14.

Garcia-Canaveras, J.C., Donato, M.T., Castell, J.V., and Lahoz, A. (2012). Targeted profiling of circulating and hepatic bile acids in human, mouse, and rat using a UPLC-MRM-MS-validated method. J Lipid Res *53*, 2231-2241.

Hassouna, R., Zizzari, P., Viltart, O., Yang, S.K., Gardette, R., Videau, C., Badoer, E., Epelbaum, J., Tolle, V. (2012). A natural variant of obestatin, Q90L, inhibits ghrelin's action on food intake and GH secretion and targets NPY and GHRH neurons in mice. PLoS One *7*, e51135.

Hebert-Chatelain, E., Desprez, T., Serrat, R., Bellocchio, L., Soria-Gomez, E., Busquets-Garcia, A., Pagano Zottola, A.C., Delamarre, A., Cannich, A., Vincent, P., Varilh, M., Robin, L.M., Terral, G., Garcia-Fernandez, M.D., Colavita, M., Mazier, W., Drago, F., Puente, N., Reguero, L., Elezgarai, I., Dupuy, J.W., Cota, D., Lopez-Rodriguez, M.L., Barreda-Gomez, G., Massa, F., Grandes, P., Benard, G., and Marsicano, G. (2016). A cannabinoid link between mitochondria and memory. Nature *539*, 555-559.

Higashi, T., Watanabe, S., Tomaru, K., Yamazaki, W., Yoshizawa, K., Ogawa, S., Nagao, H., Minato, K., Maekawa, M., and Mano, N. (2017). Unconjugated bile acids in rat brain: Analytical method based on LC/ESI-MS/MS with chemical derivatization and estimation of their origin by comparison to serum levels. Steroids *125*, 107-113.

Jensen, D.D., Godfrey, C.B., Niklas, C., Canals, M., Kocan, M., Poole, D.P., Murphy, J.E., Alemi, F., Cottrell, G.S., Korbmacher, C., Lambert, N.A., Bunnett, N.W., and Corvera, C.U. (2013). The bile acid receptor TGR5 does not interact with beta-arrestins or traffic to endosomes but transmits sustained signals from plasma membrane rafts. J Biol Chem *288*, 22942-22960.

Kawamata, Y., Fujii, R., Hosoya, M., Harada, M., Yoshida, H., Miwa, M., Fukusumi, S., Habata, Y., Itoh, T., Shintani, Y., Hinuma, S., Fujisawa, Y., and Fujino, M. (2003). A G protein-coupled receptor responsive to bile acids. J Biol Chem *278*, 9435-9440.

Keitel, V., Gorg, B., Bidmon, H.J., Zemtsova, I., Spomer, L., Zilles, K., and Haussinger, D. (2010). The bile acid receptor TGR5 (Gpbar-1) acts as a neurosteroid receptor in brain. Glia *58*, 1794-1805.

Kuipers, F., Bloks, V.W., and Groen, A.K. (2014). Beyond intestinal soap--bile acids in metabolic control. Nat Rev Endocrinol *10*, 488-498.

Kumar, D.P., Rajagopal, S., Mahavadi, S., Mirshahi, F., Grider, J.R., Murthy, K.S., and Sanyal, A.J. (2012). Activation of transmembrane bile acid receptor TGR5 stimulates insulin secretion in pancreatic beta cells. Biochem Biophys Res Commun *427*, 600-605.

Liu, S., Marcelin, G., Blouet, C., Jeong, J.H., Jo, Y.H., Schwartz, G.J., and Chua, S., Jr. (2018). A gut-brain axis regulating glucose metabolism mediated by bile acids and competitive fibroblast growth factor actions at the hypothalamus. Mol Metab *8*, 37-50.

Maruyama, T., Tanaka, K., Suzuki, J., Miyoshi, H., Harada, N., Nakamura, T., Miyamoto, Y., Kanatani, A., and Tamai, Y. (2006). Targeted disruption of G protein-coupled bile acid receptor 1 (Gpbar1/M-Bar) in mice. J Endocrinol *191*, 197-205.

McMillin, M., Frampton, G., Tobin, R., Dusio, G., Smith, J., Shin, H., Newell-Rogers, K., Grant, S., and DeMorrow, S. (2015). TGR5 signaling reduces neuroinflammation during hepatic encephalopathy. J Neurochem *135*, 565-576.

Mertens, K.L., Kalsbeek, A., Soeters, M.R., Eggink, H.M. (2017). Bile Acid Signaling Pathways from the Enterohepatic Circulation to the Central Nervous System. Front Neurosci *11*: 617.

Ockenga, J., Valentini, L., Schuetz, T., Wohlgemuth, F., Glaeser, S., Omar, A., Kasim, E., duPlessis, D., Featherstone, K., Davis, J.R., Tietge, U.J., Kroencke, T., Biebermann, H., Kohrle, J., and Brabant, G. (2012). Plasma bile acids are associated with energy expenditure and thyroid function in humans. J Clin Endocrinol Metab *97*, 535-542.

Parry, G.J., Rodrigues, C.M., Aranha, M.M., Hilbert, S.J., Davey, C., Kelkar, P., Low, W.C., and Steer, C.J. (2010). Safety, tolerability, and cerebrospinal fluid penetration of ursodeoxycholic Acid in patients with amyotrophic lateral sclerosis. Clin Neuropharmacol *33*, 17-21.

Patti, M.E., Houten, S.M., Bianco, A.C., Bernier, R., Larsen, P.R., Holst, J.J., Badman, M.K., Maratos-Flier, E., Mun, E.C., Pihlajamaki, J., Auwerx, J., and Goldfine, A.B. (2009). Serum bile acids are higher in humans with prior gastric bypass: potential contribution to improved glucose and lipid metabolism. Obesity (Silver Spring) *17*, 1671-1677.

Perino, A., Demagny, H., Velazquez-Villegas, L.A., and Schoonjans, K. (2020). Molecular Physiology of Bile Acid Signaling in Health, Disease and Aging. Physiol Rev. doi: 10.1152/physrev.00049.2019.

Perino, A., Pols, T.W., Nomura, M., Stein, S., Pellicciari, R., and Schoonjans, K. (2014). TGR5 reduces macrophage migration through mTOR-induced C/EBPbeta differential translation. J Clin Invest *124*, 5424-5436.

Quarta, C., Bellocchio, L., Mancini, G., Mazza, R., Cervino, C., Braulke, L.J., Fekete, C., Latorre, R., Nanni, C., Bucci, M., Clemens, L.E., Heldmaier, G., Watanabe, M., Leste-Lassere, T., Maitre, M., Tedesco, L., Fanelli, F., Reuss, S., Klaus, S., Srivastava, R.K., Monory, K., Valerio, A., Grandis, A., De Giorgio, R., Pasquali, R., Nisoli, E., Cota, D., Lutz, B., Marsicano, G., and Pagotto, U. (2010). CB(1) signaling in forebrain and sympathetic neurons is a key determinant of endocannabinoid actions on energy balance. Cell Metab *11*, 273-285.

Saucisse, N., Mazier, W., Simon, V., Binder, E., Catania., C., Bellocchio, L., Romanov, R.A., Matias,I., Zizzari, P., Leon, S., Quarta, C., Cannich, A., Meece, K., Gonzales, D., Clark, S., Becker, J.M., Yeo, G.S.H., Merkle F.T., Wardlaw S.L., Harkany, T., Massa, F., Marsicano, G., Cota, D. (2020). POMC neurons functional heterogeneity relies on mTORC1 signaling. bioRxiv 2020.03.25.007765; doi:10.1101/2020.03.25.007765.

Schwenk, F., Baron, U., and Rajewsky, K. (1995). A cre-transgenic mouse strain for the ubiquitous deletion of loxP-flanked gene segments including deletion in germ cells. Nucleic Acids Res *23*, 5080-5081.

Simonen, M., Dali-Youcef, N., Kaminska, D., Venesmaa, S., Kakela, P., Paakkonen, M., Hallikainen, M., Kolehmainen, M., Uusitupa, M., Moilanen, L., Laakso, M., Gylling, H., Patti, M.E., Auwerx, J., and Pihlajamaki, J. (2012). Conjugated bile acids associate with altered rates of glucose and lipid oxidation after Roux-en-Y gastric bypass. Obes Surg *22*, 1473-1480.

Song, P., Zhang, Y., and Klaassen, C.D. (2011). Dose-response of five bile acids on serum and liver bile Acid concentrations and hepatotoxicty in mice. Toxicol Sci *123*, 359-367.

Teodoro, J.S., Zouhar, P., Flachs, P., Bardova, K., Janovska, P., Gomes, A.P., Duarte, F.V., Varela, A.T., Rolo, A.P., Palmeira, C.M., and Kopecky, J. (2014). Enhancement of brown fat thermogenesis using chenodeoxycholic acid in mice. Int J Obes (Lond) *38*, 1027-1034.

Thomas, C., Gioiello, A., Noriega, L., Strehle, A., Oury, J., Rizzo, G., Macchiarulo, A., Yamamoto, H., Mataki, C., Pruzanski, M., Pellicciari, R., Auwerx, J., and Schoonjans,

K. (2009). TGR5-mediated bile acid sensing controls glucose homeostasis. Cell Metab *10*, 167-177.

Tremaroli, V., Karlsson, F., Werling, M., Ståhlman, M., Kovatcheva-Datchary, P., Olbers, T., Fändriks, L., le Roux, C.W., Nielsen, J., Bäckhed, F. (2015). Roux-en-Y Gastric Bypass and Vertical Banded Gastroplasty Induce Long-Term Changes on the Human Gut Microbiome Contributing to Fat Mass Regulation. Cell Metab *22*, 228-238.

Vaughan, C.H., Zarebidaki, E., Ehlen, J.C., and Bartness, T.J. (2014). Analysis and measurement of the sympathetic and sensory innervation of white and brown adipose tissue. Methods Enzymol *537*, 199-225.

Velazquez-Villegas, L.A., Perino, A., Lemos, V., Zietak, M., Nomura, M., Pols, T.W.H., and Schoonjans, K. (2018). TGR5 signalling promotes mitochondrial fission and beige remodelling of white adipose tissue. Nat Commun *9*, 245.

Watanabe, M., Houten, S.M., Mataki, C., Christoffolete, M.A., Kim, B.W., Sato, H., Messaddeq, N., Harney, J.W., Ezaki, O., Kodama, T., Schoonjans, K., Bianco, A.C., and Auwerx, J. (2006). Bile acids induce energy expenditure by promoting intracellular thyroid hormone activation. Nature *439*, 484-489.

Wu, X., Li, J.Y., Lee, A., Lu, Y.X., Zhou, S.Y., and Owyang, C. (2020). Satiety induced by bile acids is mediated via vagal afferent pathways. JCI Insight *5*.

Zietak, M., and Kozak, L.P. (2016). Bile acids induce uncoupling protein 1-dependent thermogenesis and stimulate energy expenditure at thermoneutrality in mice. Am J Physiol Endocrinol Metab *310*, E346-354.

Zuo, G., Zhang, T., Huang, L., Araujo, C., Peng, J., Travis, Z., Okada, T., Ocak, U., Zhang, G., Tang, J., Lu, X., and Zhang, J.H. (2019). Activation of TGR5 with INT-777 attenuates oxidative stress and neuronal apoptosis via cAMP/PKCepsilon/ALDH2 pathway after subarachnoid hemorrhage in rats. Free Radic Biol Med *143*, 441-453.

Figure 1

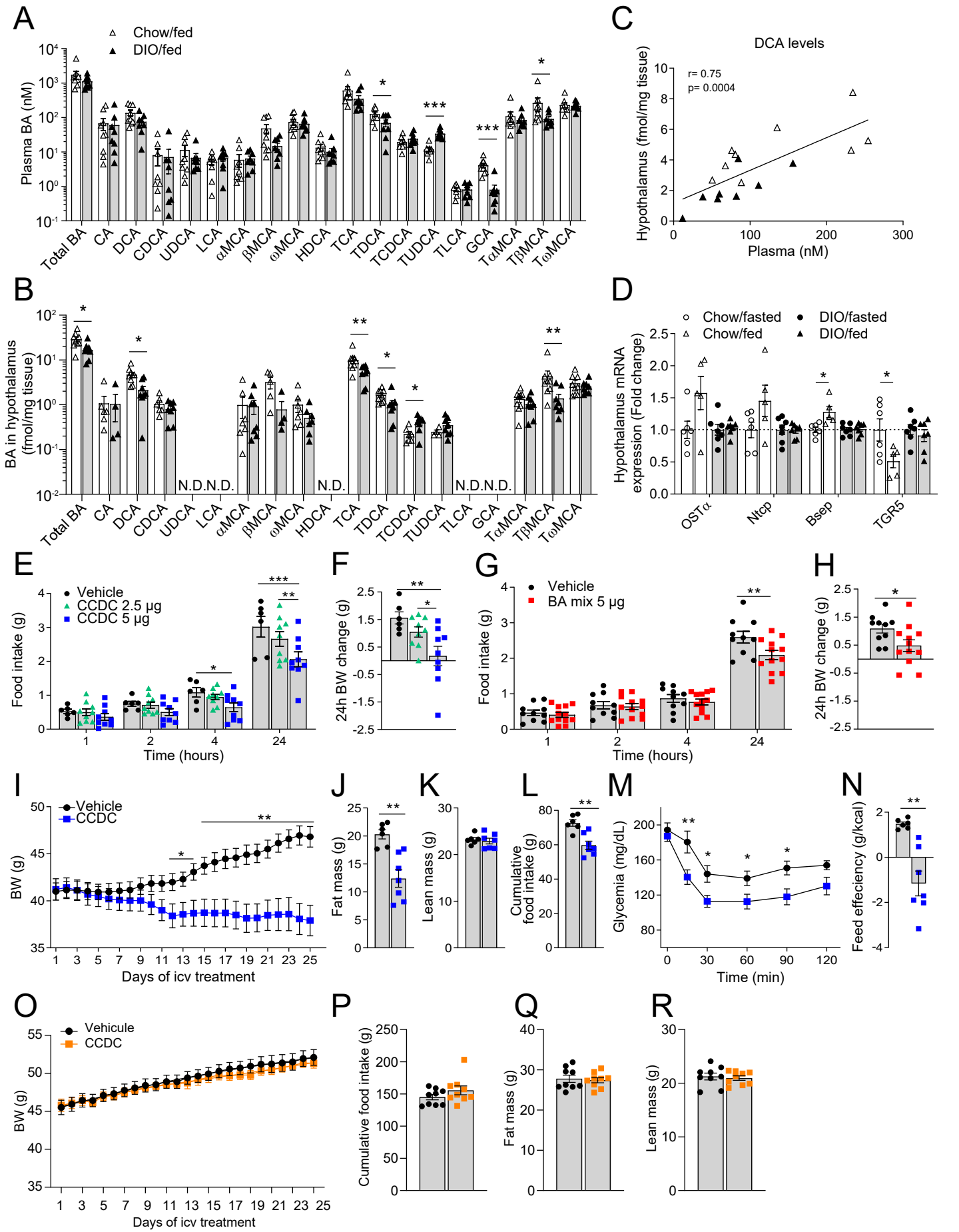
A
Chow/fed
DIO/fed
Plasma BA (nM)
Total BA
CA
DCA
CDCA
UDCA
LCA
αMCA
βMCA
ωMCA
HDCA
TCA
TDCA
TCDCA
TUDCA
TLCA
GCA
TαMCA
TβMCA
TωMCA
B
BA in hypothalamus (fmol/mg tissue)
N.D.
C
DCA levels
r= 0.75
p= 0.0004
Hypothalamus (fmol/mg tissue)
Plasma (nM)
D
Chow/fasted
Chow/fed
DIO/fasted
DIO/fed
Hypothalamus mRNA expression (Fold change)
OSTα
Ntcp
Bsep
TGR5
E
Vehicle
CCDC 2.5 µg
CCDC 5 µg
Food intake (g)
Time (hours)
F
24h BW change (g)
G
Vehicle
BA mix 5 µg
Food intake (g)
Time (hours)
H
24h BW change (g)
I
Vehicle
CCDC
BW (g)
Days of icv treatment
J
Fat mass (g)
K
Lean mass (g)
L
Cumulative food intake (g)
M
Glycemia (mg/dL)
Time (min)
N
Feed effeciency (g/kcal)
O
Vehicule
CCDC
BW (g)
Days of icv treatment
P
Cumulative food intake (g)
Q
Fat mass (g)
R
Lean mass (g)

Figure 2

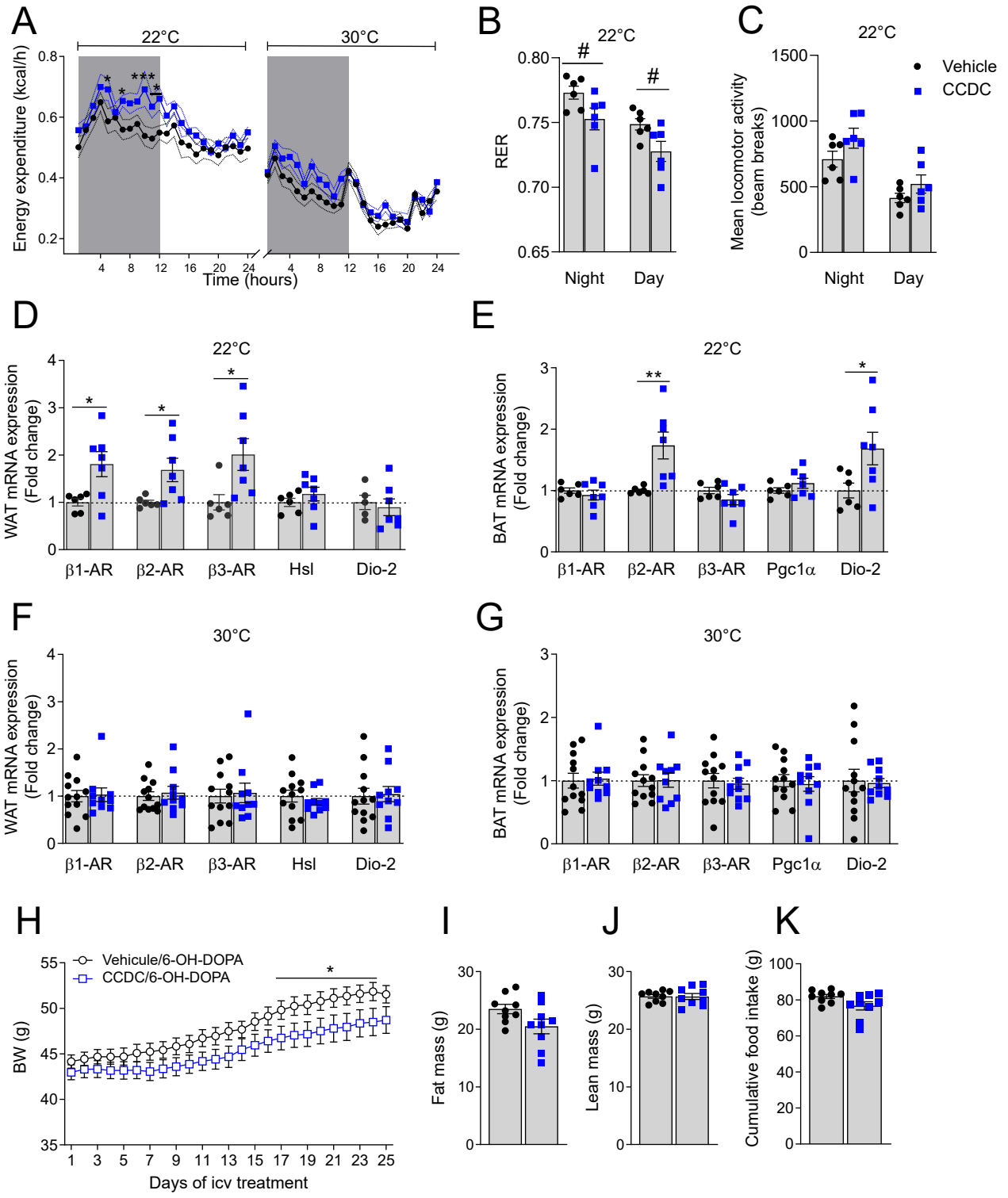
A
22°C
30°C
Energy expenditure (kcal/h)
Time (hours)
B
22°C
RER
Night
Day
C
22°C
Mean locomotor activity (beam breaks)
Vehicle
CCDC
Night
Day
D
22°C
WAT mRNA expression (Fold change)
β1-AR
β2-AR
β3-AR
Hsl
Dio-2
E
22°C
BAT mRNA expression (Fold change)
β1-AR
β2-AR
β3-AR
Pgc1α
Dio-2
F
30°C
WAT mRNA expression (Fold change)
β1-AR
β2-AR
β3-AR
Hsl
Dio-2
G
30°C
BAT mRNA expression (Fold change)
β1-AR
β2-AR
β3-AR
Pgc1α
Dio-2
H
Vehicule/6-OH-DOPA
CCDC/6-OH-DOPA
BW (g)
Days of icv treatment
I
Fat mass (g)
J
Lean mass (g)
K
Cumulative food intake (g)

Figure 3

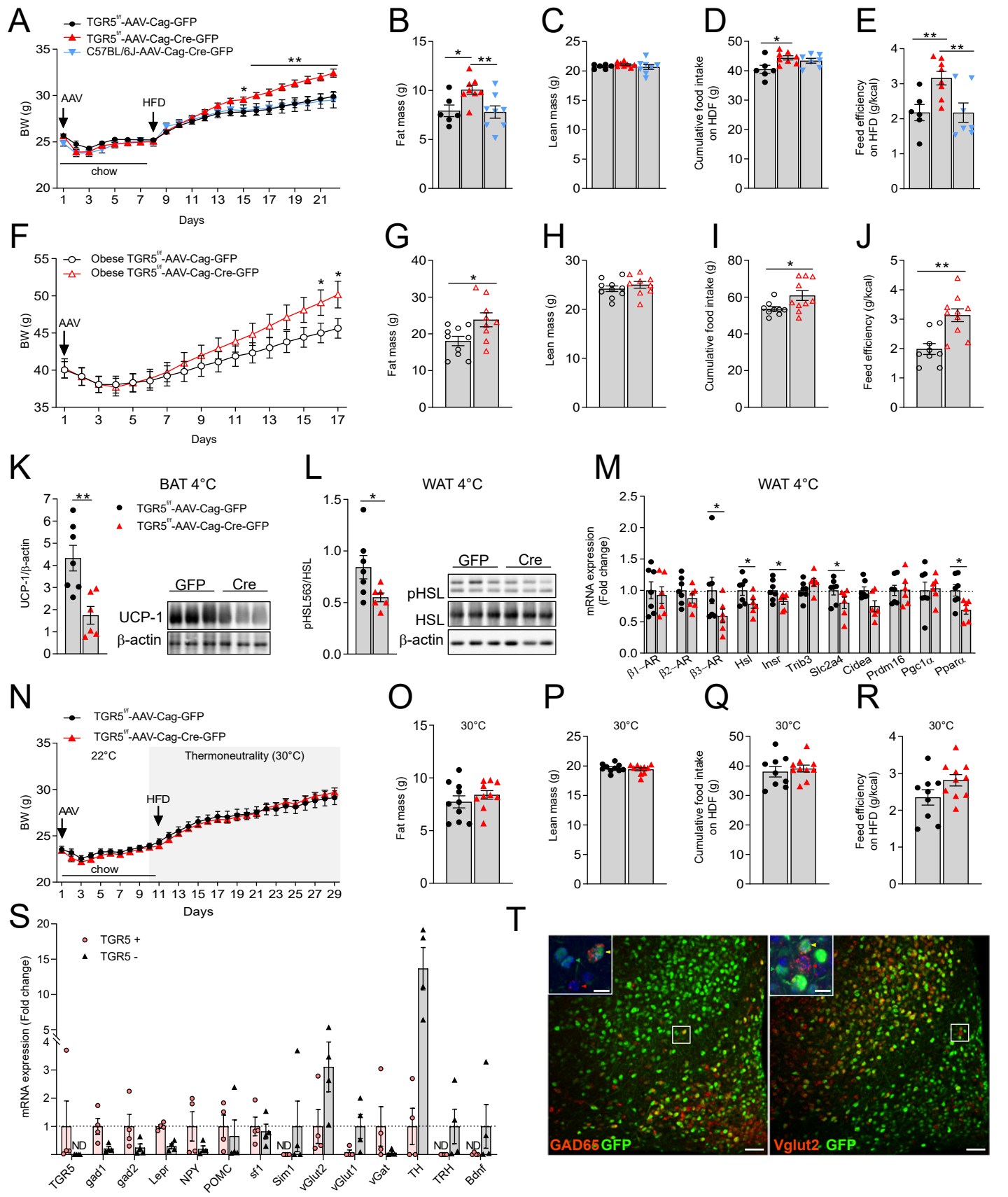
A
TGR5f/f-AAV-Cag-GFP
TGR5f/f-AAV-Cag-Cre-GFP
C57BL/6J-AAV-Cag-Cre-GFP
AAV
HFD
chow
BW (g)
Days
B
Fat mass (g)
C
Lean mass (g)
D
Cumulative food intake on HDF (g)
E
Feed efficiency on HFD (g/kcal)
F
Obese TGR5f/f-AAV-Cag-GFP
Obese TGR5f/f-AAV-Cag-Cre-GFP
AAV
BW (g)
Days
G
Fat mass (g)
H
Lean mass (g)
I
Cumulative food intake (g)
J
Feed efficiency (g/kcal)
K
BAT 4°C
TGR5f/f-AAV-Cag-GFP
TGR5f/f-AAV-Cag-Cre-GFP
UCP-1/β-actin
GFP
Cre
UCP-1
β-actin
L
WAT 4°C
pHSL563/HSL
GFP
Cre
pHSL
HSL
β-actin
M
WAT 4°C
mRNA expression (Fold change)
β1–AR
β2–AR
β3–AR
Hsl
Insr
Trib3
Slc2a4
Cidea
Prdm16
Pgc1α
Pparα
N
TGR5f/f-AAV-Cag-GFP
TGR5f/f-AAV-Cag-Cre-GFP
22°C
Thermoneutrality (30°C)
AAV
HFD
chow
BW (g)
Days
O
30°C
Fat mass (g)
P
30°C
Lean mass (g)
Q
30°C
Cumulative food intake on HDF (g)
R
30°C
Feed efficiency on HFD (g/kcal)
S
TGR5 +
TGR5 -
mRNA expression (Fold change)
ND
TGR5
gad1
gad2
Lepr
NPY
POMC
sf1
Sim1
vGlut2
vGlut1
vGat
TH
TRH
Bdnf
T
GAD65 GFP
Vglut2 GFP

Figure 4

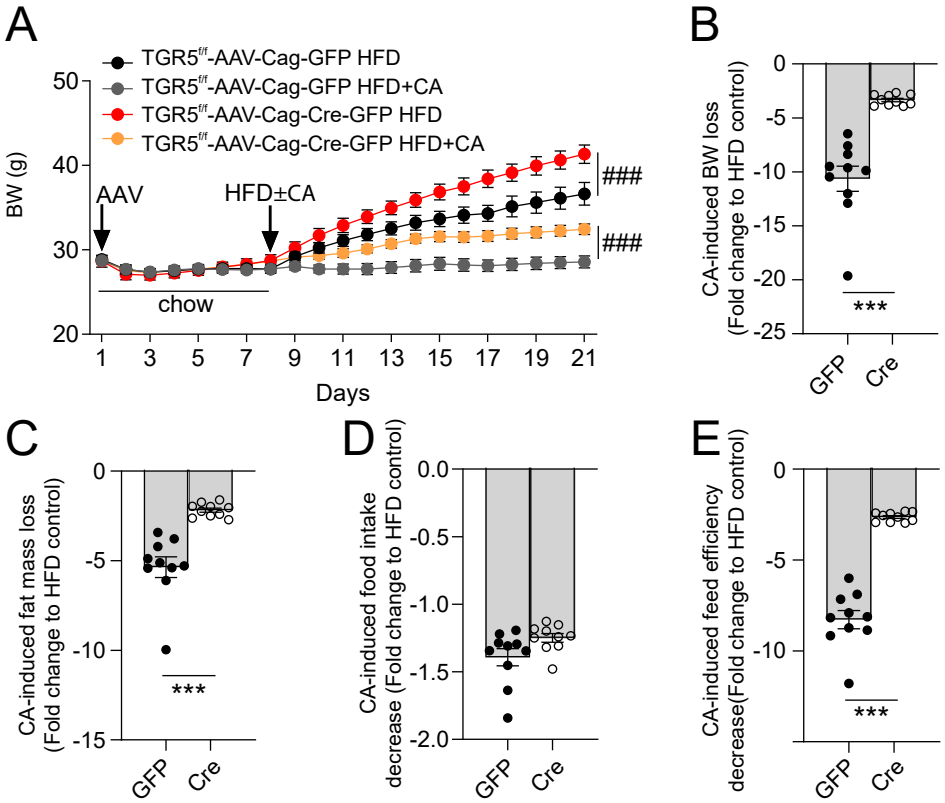
A
TGR5f/f-AAV-Cag-GFP HFD
TGR5f/f-AAV-Cag-GFP HFD+CA
TGR5f/f-AAV-Cag-Cre-GFP HFD
TGR5f/f-AAV-Cag-Cre-GFP HFD+CA
BW (g)
AAV
HFD±CA
chow
###
###
Days
B
CA-induced BW loss
(Fold change to HFD control)
***
GFP
Cre
C
CA-induced fat mass loss
(Fold change to HFD control)
***
GFP
Cre
D
CA-induced food intake
decrease (Fold change to HFD control)
GFP
Cre
E
CA-induced feed efficiency
decrease(Fold change to HFD control)
***
GFP
Cre

Figure S1

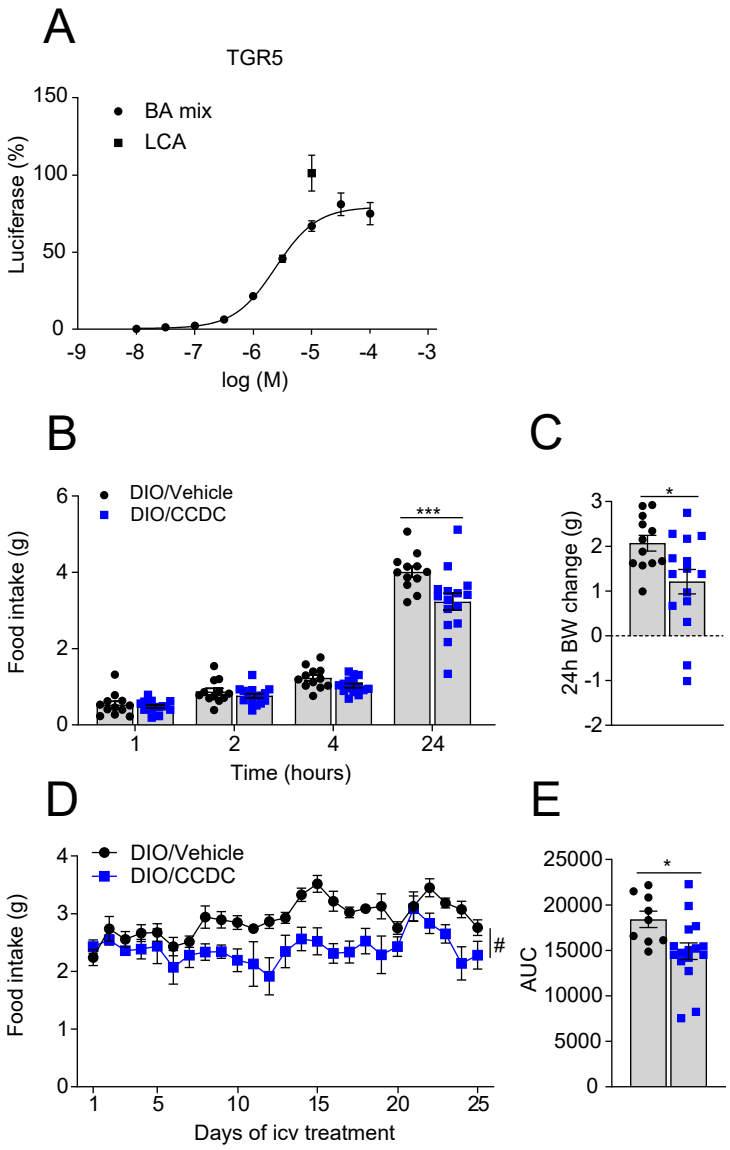
A
TGR5
BA mix
LCA
Luciferase (%)
150
100
50
0
-9
-8
-7
-6
-5
-4
-3
log (M)
B
DIO/Vehicle
DIO/CCDC
Food intake (g)
6
4
2
0
***
1
2
4
24
Time (hours)
C
24h BW change (g)
3
2
1
0
-1
-2
*
D
DIO/Vehicle
DIO/CCDC
Food intake (g)
4
3
2
1
0
#
1
5
10
15
20
25
Days of icv treatment
E
AUC
25000
20000
15000
10000
5000
0
*

Figure S2

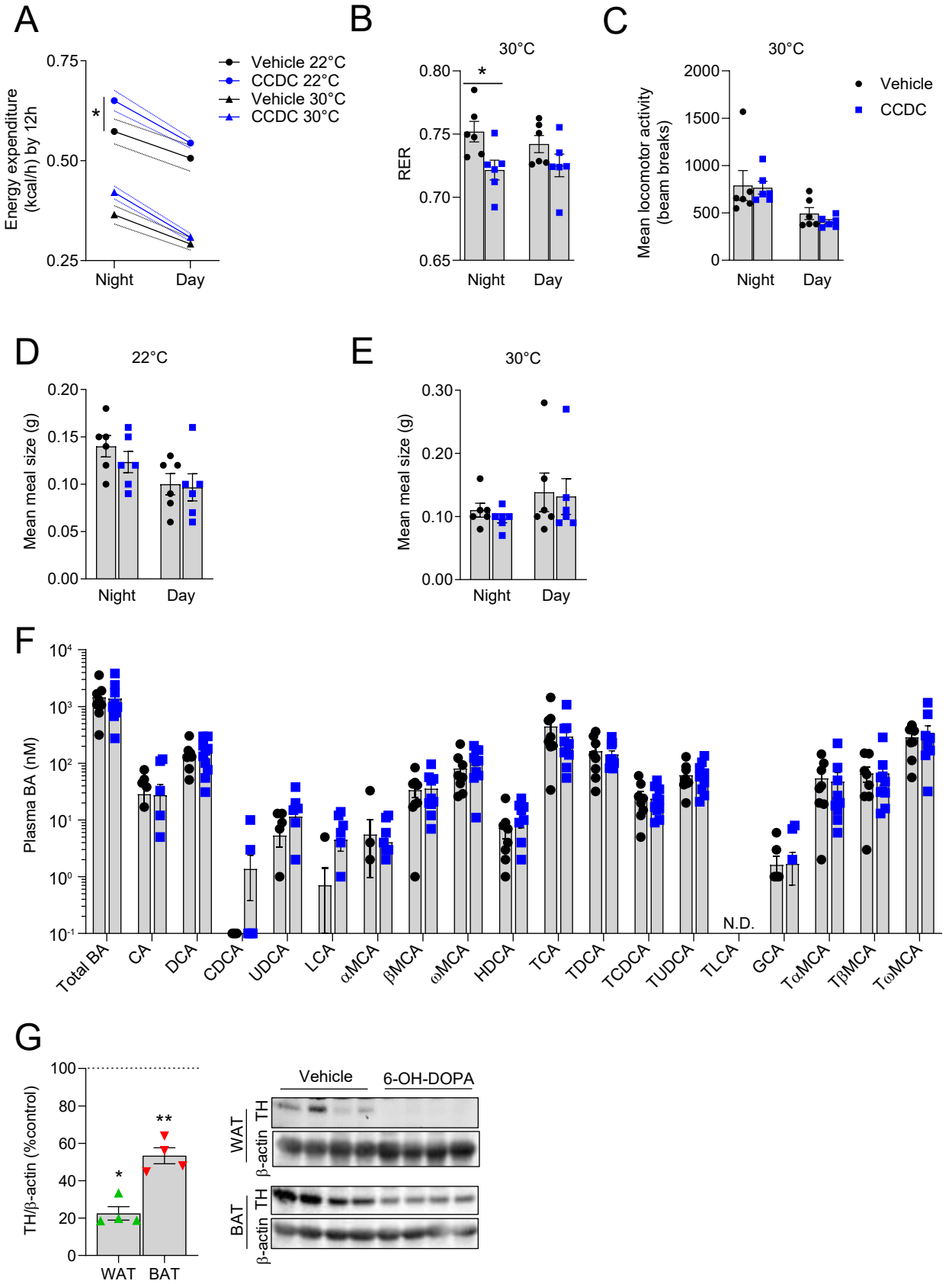
A
Energy expenditure (kcal/h) by 12h
0.75
0.50
0.25
*
Night
Day
Vehicle 22°C
CCDC 22°C
Vehicle 30°C
CCDC 30°C
B
30°C
RER
0.80
0.75
0.70
0.65
*
Night
Day
C
30°C
Mean locomotor activity (beam breaks)
2000
1500
1000
500
0
Night
Day
Vehicle
CCDC
D
22°C
Mean meal size (g)
0.20
0.15
0.10
0.05
0.00
Night
Day
E
30°C
Mean meal size (g)
0.30
0.20
0.10
0.00
Night
Day
F
Plasma BA (nM)
10^4
10^3
10^2
10^1
10^0
10^{-1}
N.D.
Total BA
CA
DCA
CDCA
UDCA
LCA
αMCA
βMCA
ωMCA
HDCA
TCA
TDCA
TCDCA
TUDCA
TLCA
GCA
TαMCA
TβMCA
TωMCA
G
TH/β-actin (%control)
100
80
60
40
20
0
*
**
WAT
BAT
Vehicle
6-OH-DOPA
WAT
TH
β-actin
BAT
TH
β-actin

Figure S3

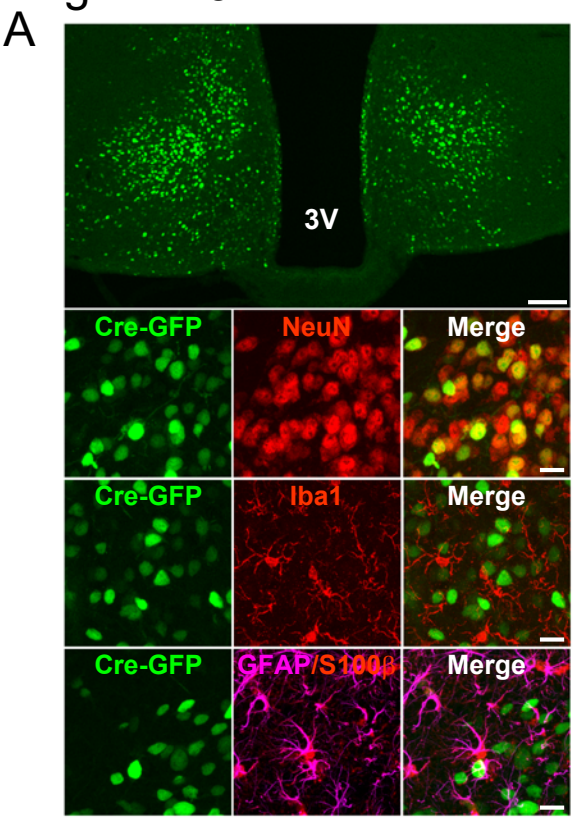
A
3V
Cre-GFP
NeuN
Merge
Cre-GFP
Iba1
Merge
Cre-GFP
GFAP/S100β
Merge

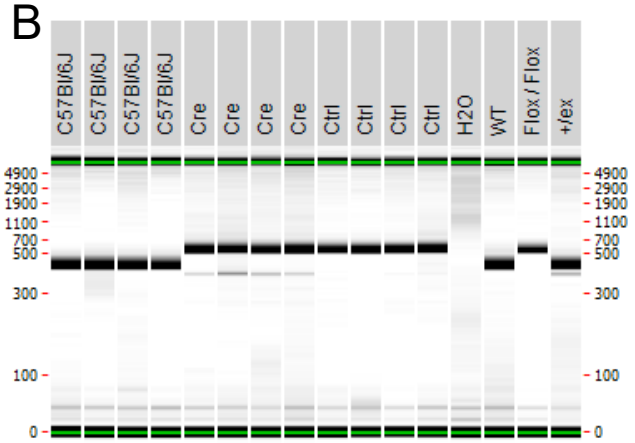
B
C57Bl/6J
C57Bl/6J
C57Bl/6J
C57Bl/6J
Cre
Cre
Cre
Cre
Ctrl
Ctrl
Ctrl
Ctrl
H2O
WT
Flox / Flox
+/ex
4900
2900
1900
1100
700
500
300
100
0

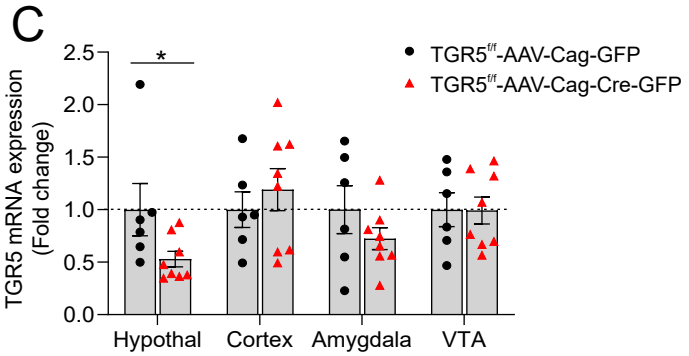
C
TGR5 mRNA expression (Fold change)
2.5
2.0
1.5
1.0
0.5
0.0
*
TGR5f/f-AAV-Cag-GFP
TGR5f/f-AAV-Cag-Cre-GFP
Hypothal
Cortex
Amygdala
VTA

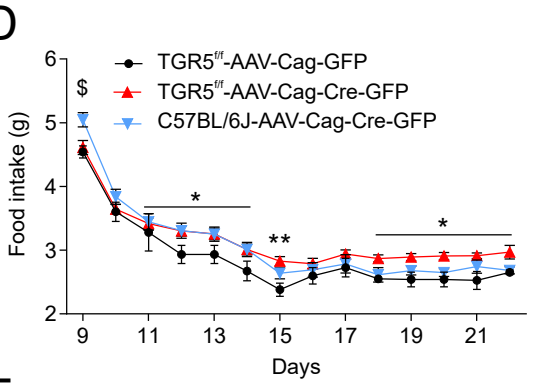
D
Food intake (g)
6
5
4
3
2
$
*
**
*
TGR5f/f-AAV-Cag-GFP
TGR5f/f-AAV-Cag-Cre-GFP
C57BL/6J-AAV-Cag-Cre-GFP
9
11
13
15
17
19
21
Days

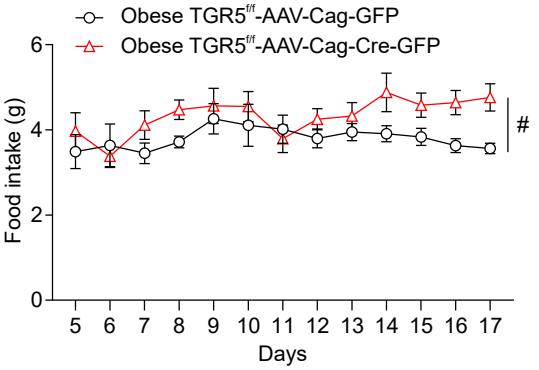
E
Obese TGR5f/f-AAV-Cag-GFP
Obese TGR5f/f-AAV-Cag-Cre-GFP
Food intake (g)
6
4
2
0
#
5
6
7
8
9
10
11
12
13
14
15
16
17
Days

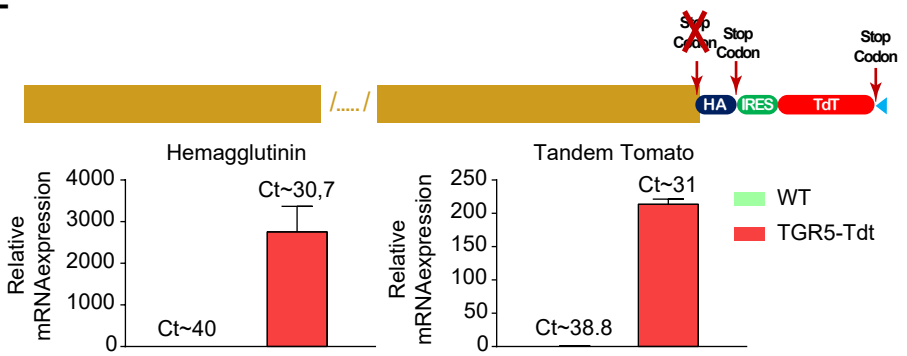
F
Stop Codon
Stop Codon
Stop Codon
/...../
HA
IRES
TdT
Hemagglutinin
Relative mRNAexpression
4000
3000
2000
1000
0
Ct~30,7
Ct~40
Tandem Tomato
Relative mRNAexpression
250
200
150
100
50
0
Ct~31
Ct~38.8
WT
TGR5-Tdt

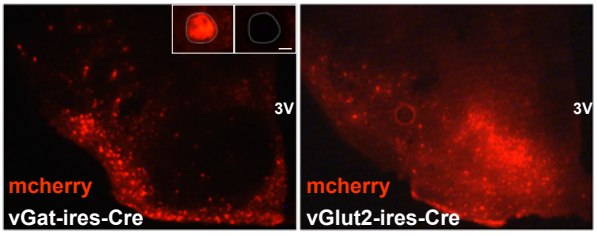
G
3V
mcherry
vGat-ires-Cre
3V
mcherry
vGlut2-ires-Cre

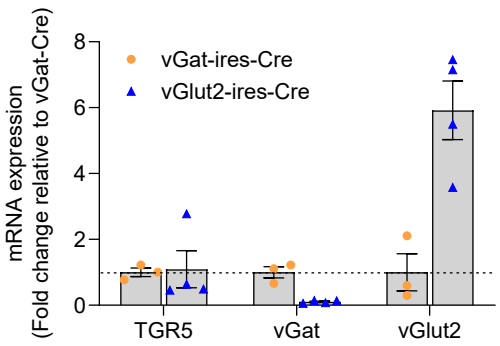
H
mRNA expression (Fold change relative to vGat-Cre)
8
6
4
2
0
vGat-ires-Cre
vGlut2-ires-Cre
TGR5
vGat
vGlut2

Figure S4

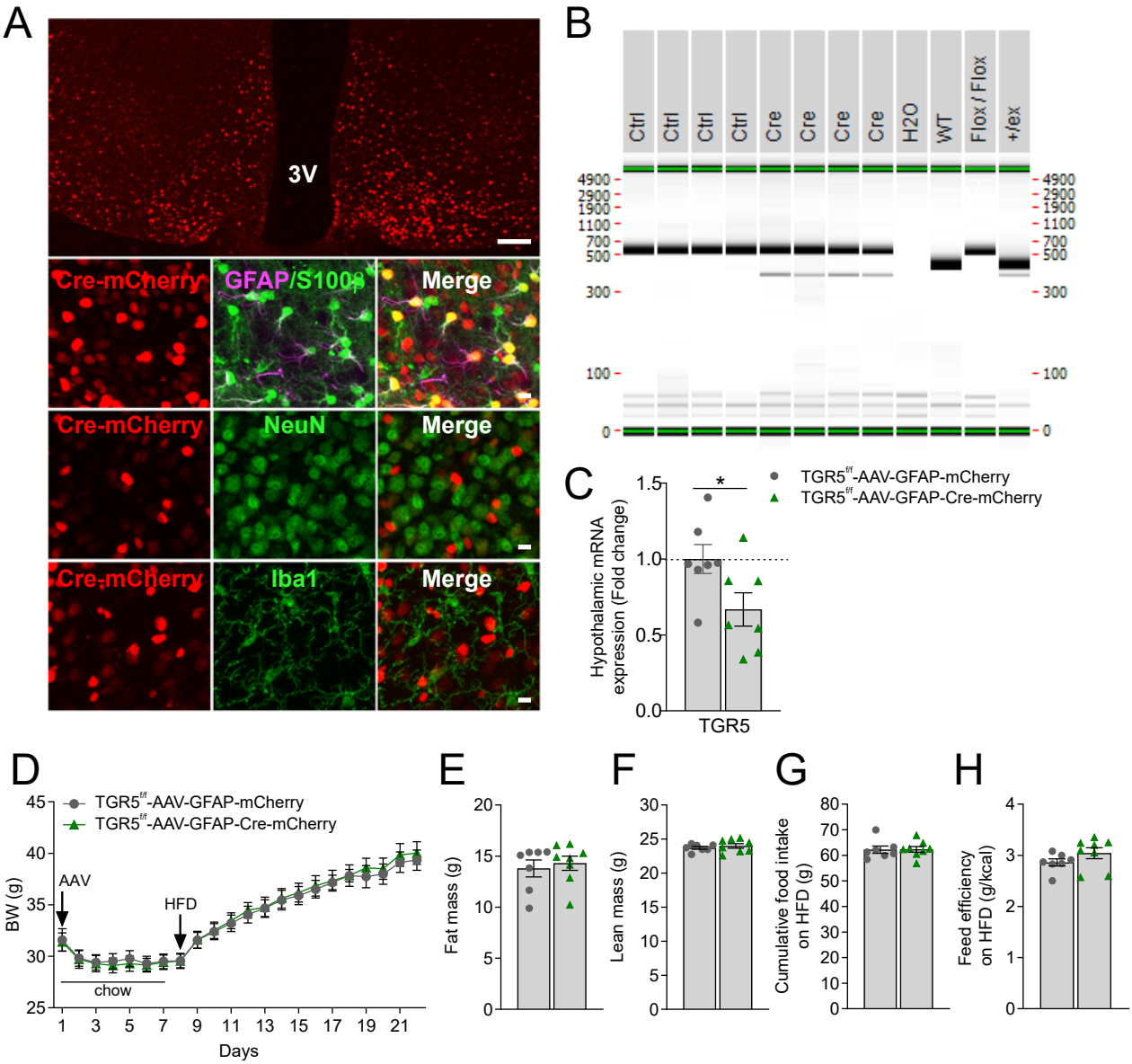
A
3V
Cre-mCherry
GFAP/S100β
Merge
Cre-mCherry
NeuN
Merge
Cre-mCherry
Iba1
Merge
B
Ctrl
Ctrl
Ctrl
Ctrl
Cre
Cre
Cre
Cre
H2O
WT
Flox / Flox
+/ex
4900
2900
1900
1100
700
500
300
100
0
C
TGR5f/f-AAV-GFAP-mCherry
TGR5f/f-AAV-GFAP-Cre-mCherry
Hypothalamic mRNA expression (Fold change)
1.5
1.0
0.5
0.0
*
TGR5
D
TGR5f/f-AAV-GFAP-mCherry
TGR5f/f-AAV-GFAP-Cre-mCherry
BW (g)
AAV
HFD
chow
Days
E
Fat mass (g)
F
Lean mass (g)
G
Cumulative food intake on HFD (g)
H
Feed efficiency on HFD (g/kcal)

Figure S5

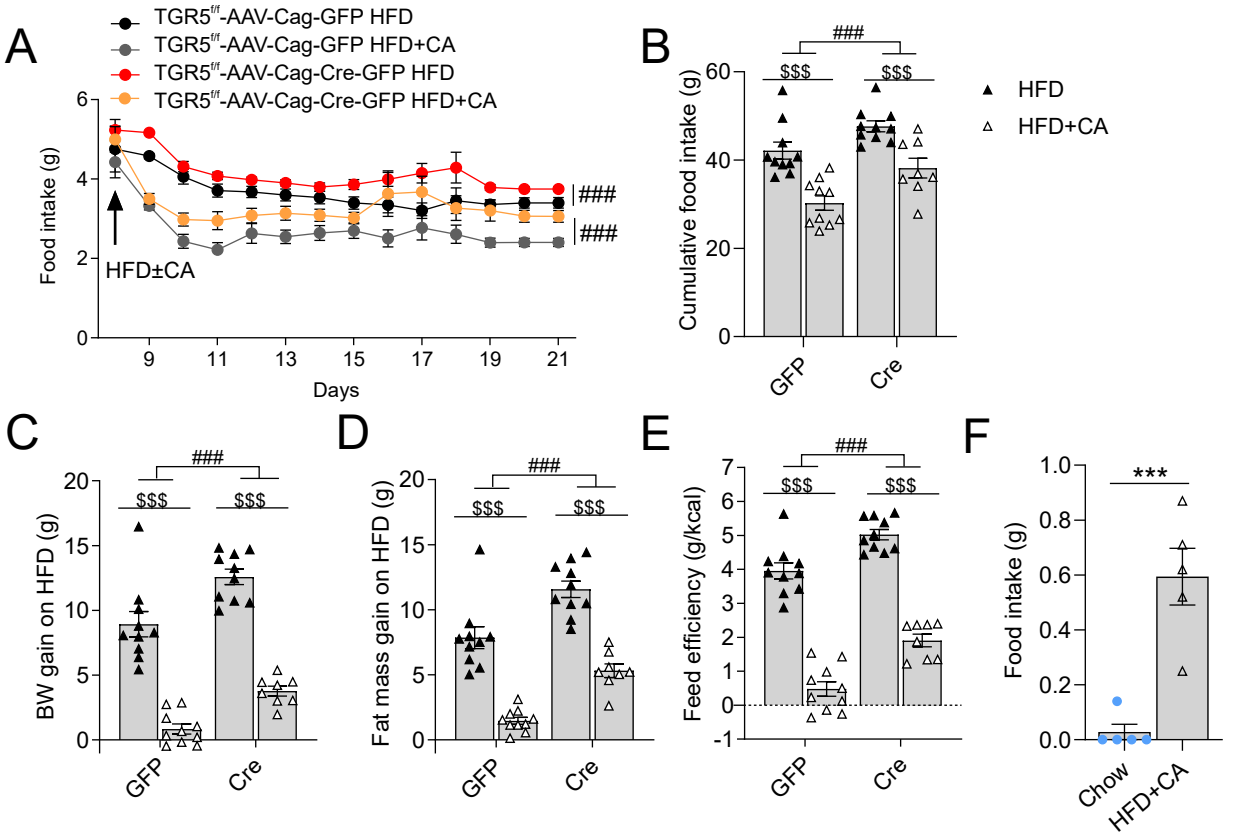
A
TGR5f/f-AAV-Cag-GFP HFD
TGR5f/f-AAV-Cag-GFP HFD+CA
TGR5f/f-AAV-Cag-Cre-GFP HFD
TGR5f/f-AAV-Cag-Cre-GFP HFD+CA
Food intake (g)
HFD±CA
###
###
Days
B
Cumulative food intake (g)
###
$$$
$$$
HFD
HFD+CA
GFP
Cre
C
BW gain on HFD (g)
D
Fat mass gain on HFD (g)
E
Feed efficiency (g/kcal)
F
Food intake (g)
***
Chow
HFD+CA